6. Cooperative Programs

Facilitating a View of Energy Deposition in the Neutral Atmosphere

GAIL ANDERSON
Air Force Research Laboratory/Space Vehicles Directorate, U.S. Air Force, Boulder, Colorado 80503-3328

ALEXANDER BERK
Spectral Sciences Inc., Burlington, Massachusetts 01803-3304

JOYCE HARRIS AND ELLSWORTH DUTTON
NOAA CMDL, Boulder, Colorado 80503-3328

ALLEN JORDAN, ROBERT STONE, AND ELIZABETH ANDREWS
Cooperative Institute for Research in Environmental Sciences, Boulder, Colorado 80309-0216

ERIC SHETTLE
U. S. Naval Research Laboratory, S. W., Washington, D. C. 20375

Active collaboration between the Climate Monitoring and Diagnostics Laboratory (CMDL) and the U.S. Air Force Research Laboratory (AFRL) facilitates cross-validation of measurement and radiative transfer (RT) modeling. The research efforts are driven by CMDL's need to model the radiative components of its measurements and the AFRL's need to test the theoretical underpinnings of its RT algorithms, particularly the Moderate Resolution Transmittance (MODTRAN) code [*Anderson et al*., 2000]. In 2002 and 2003 the research focused on the study of the impacts of Asian dust events, particularly as the dust clouds migrate over the Arctic. The primary impact of the dust layer can be addressed solely by examining its radiative properties relative to the underlying snow and intervening pristine background environment. Through a sequence of ground-based visibility measurements of the aerosols coupled with lidar measurements of the layer height, CMDL was able to provide appropriate input parameters for a suite of MODTRAN calculations that integrated forcing at the surface along with estimates of the local heating/cooling at altitude, with and without the dust cloud. This led to a closure experiment where MODTRAN predictions of surface forcing were in remarkably good agreement with the CMDL measurements for a set of solar zenith angles and aerosol optical depths (see "Closure Experiment" on page 88 for additional information).

The process of adapting MODTRAN to this particular study required two important upgrades. The first involved how to best define a realistic aerosol layer in which the standard aerosol optical properties (attenuation coefficient, extinction coefficient, and single scattering albedo) are each given as a function of wavelength. Previously, MODTRAN required all aerosols to fit into a very simplistic altitude configuration defined by only four layer types. The measured Asian dust cloud required more flexibility with respect to defining the cloud's density profile, along with its optical properties, as a function of altitude. That flexibility is available now as a user-defined option. The second and more important contribution to MODTRAN, however, is the ability to depict the relative heating and cooling (flux divergence) for all the atmospheric layers (surface to ~80 km), as a function of wavelength or frequency. The spectral range is selectable and may be inclusive of the entire MODTRAN spectral range from the UV to the far-infrared (IR) (0.2 to ~40 mm). Using this tool, the potential impact of the dust cloud can readily be compared to a clear sky scenario. A new code was written by a CMDL team to facilitate the creation of plots and spectral integration as a function of altitude (Figures 1, 2, and 3).

This capability will be released as an Interactive Data Language (IDL™) executable code that only requires the MODTRAN calculations to produce compatible cooling rate (*.clr) files. This plotting package will become the first non-AFRL code to be delivered with the MODTRAN software. Without access to the quality of the CMDL measurements and associated campaigns, this new ability to employ MODTRAN for climate-related studies would be severely limited and negatively impacted.

There are obvious extensions associated with flux-divergence studies. In general, the heating rate can be defined by:

$$\left(\frac{\Delta T}{\Delta t}\right)_{total} = \frac{g}{C_p}\frac{F(p) - F(p - \Delta p)}{\Delta p}$$

where:

$\Delta T/\Delta t$ = Temperature increment for time interval t,
g = gravitational constant (z),
C_p = specific heat at constant pressure,
$F(p)$ = Net Flux at layer boundary (p), and
p = pressure level.

Expanding the altitude scale below 100 mb provides a more detailed view of the radiometric impact of the dust cloud. The ability to examine and manipulate the data in this visual manner will permit a broader understanding of the physics of the atmosphere and any potential inadequacies of the MODTRAN formulations. Of particular concern are the very small (<1.e-4K day^{-1}) layers of cooling at the dust-cloud boundaries; this may well be an artifact of the very abrupt dust cloud boundaries at 2 and 4 km.

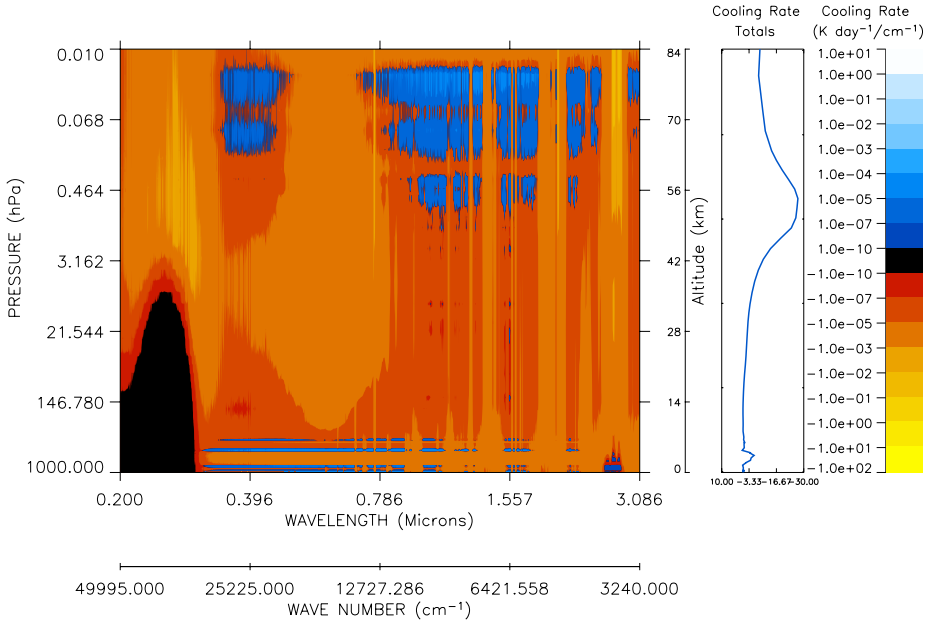

Figure 1. Cooling rate image generated from a MODTRAN cooling rate file (*.clr). Yellow-to-red denotes heating, while blue-to-white denotes cooling. This spectral range includes only the solar source function, between 0.2 and 3 µm. The ozone heating near 50 km is the dominant feature. The Asian dust cloud contribution can be seen between the surface and ~5 km. The integrated cooling (K day^{-1}) is also provided. [NOTE: The black region in the UV is the solar blind region where no solar photons can penetrate.]

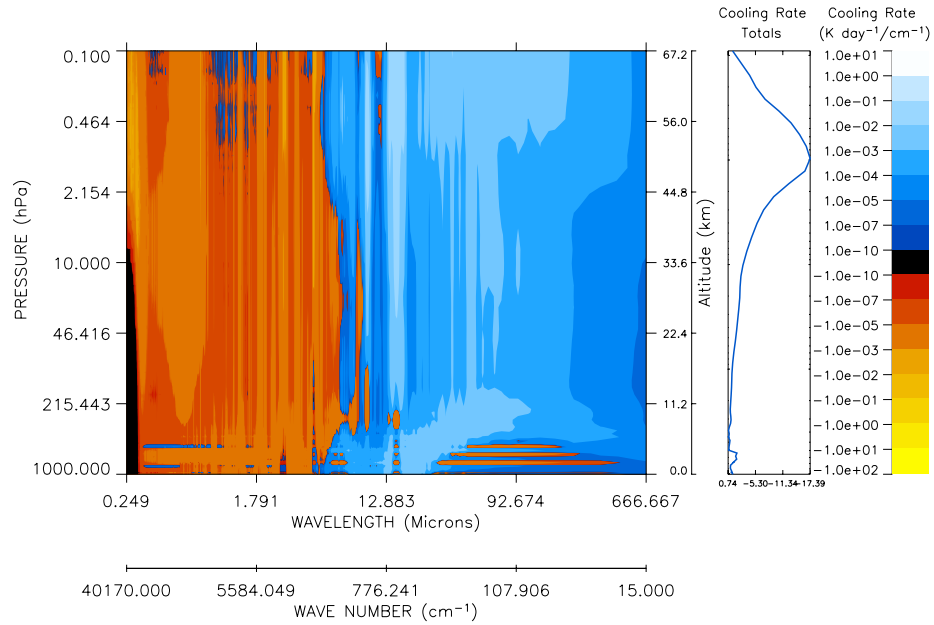

Figure 2. Cooling rate image generated from the same MODTRAN cooling rate file with the same color scale as in Figure 1. The net stratospheric heating is now a combination of O_3 solar heating in the UV (~30 K day^{-1}, as in Figure 1) and the thermal cooling to space in both the 9.6 µm O_3 and 15 µm CO_2 bands (~ -3 and -10 K day^{-1}, respectively), produce a net heating of ~15 K day^{-1} at the stratopause.

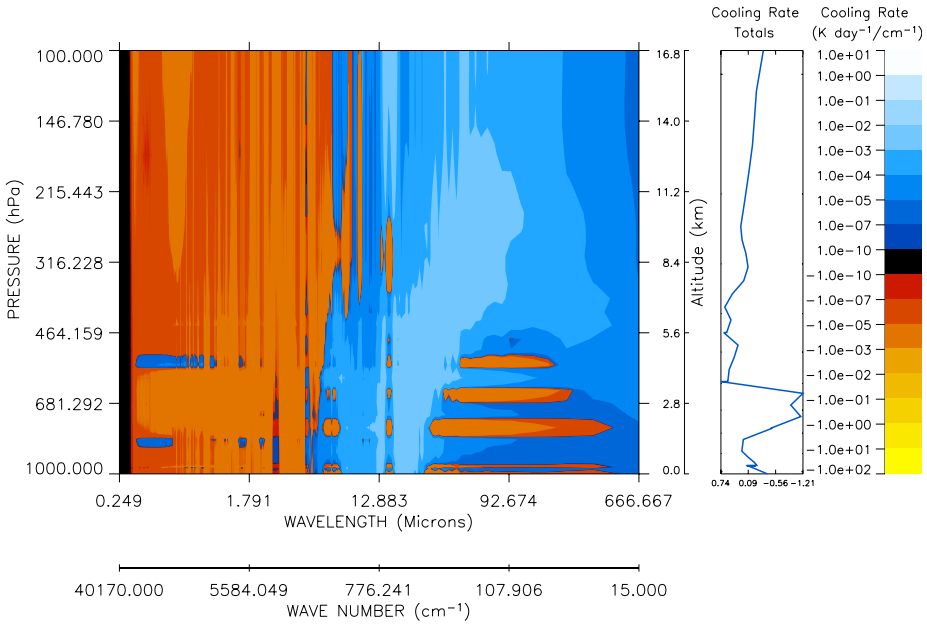

Figure 3. Cooling rate image generated from the same MODTRAN flux-divergence file (*.clr) as in Figure 2. The net heating of the dust cloud is ~2 K day^{-1}, where the vertical extent of the cloud (between 2 and 4 km) was based on actual lidar observations. Because of the wavelength scale, the important 9.6 µm O_3 and 15 µm CO_2 bands were visually compressed.

REFERENCE

Anderson, G.P., A. Berk, P.K. Acharya, M.W. Matthew, L.S. Bernstein, J.H. Chetwynd, H. Dothe, S.M. Adler-Golden, A.J. Ratkowski, G.W. Felde, J.A. Gardner, M.L. Hoke, S.C. Richtsmeier, B. Pukall, J. Mello and L.S. Jeong (2000), MODTRAN4: Radiative transfer modeling for remote sensing in algorithms for multispectral, hyperspectral, and ultraspectral imagery VI, edited by S. Chen and M. R. Descour, *Procceedings of SPIE 4049-16*, pp. 176-183, Int. Soc. Opt. Eng., Orlando, FL, 24 April 2000.

UV Spectroradiometer Monitoring Program: Spectral Global Irradiance and Total Column Ozone Measurements at South Pole and Barrow

G. BERNHARD, C. R. BOOTH, AND J. C. EHRAMJIAN
Biospherical Instruments Inc., San Diego, California 92110-2621

INTRODUCTION

The United States National Science Foundation's Office of Polar Programs (NSF/OPP) Ultraviolet Spectroradiometer Monitoring Network was established in 1988 to collect data on the consequences of ozone depletion. The network currently consists of six automated, high-resolution spectroradiometers (Table 1). Three are located in Antarctica, including one at the CMDL South Pole Observatory (SPO). Another instrument is deployed close to the CMDL Barrow Observatory (BRW). Now in its sixteenth year of operation, the network continues to make measurements of ultraviolet (UV) spectral irradiance and provides a variety of data products to quantify biologically relevant UV exposures. Biospherical Instruments Inc. is responsible for operating the network and distributing its data to the scientific community.

The network is equipped with Biospherical Instruments Inc. model SUV-100 spectroradiometers. Each instrument contains a double monochromator with holographic gratings and a photomultiplier tube detector. Spectra are sampled automatically every 15 minutes between 280 and 600 nm with a spectral bandwidth of 1.0 nm full width at half maximum (FWHM). Tungsten-halogen and mercury-vapor calibration lamps are used for daily automatic calibrations of responsivity and wavelength registration. All instrument functions, calibration activities, and solar data acquisition are computer controlled. Further details on the spectroradiometers are described in the work of *Booth et al.* [1994] and *Bernhard et al.* [2003a]. Network data, operations reports, and publications can be accessed via the project's Web site www.biospherical.com/NSF.

UV RADIATION CLIMATE AT SPO AND BRW

SPO is a unique place for UV measurements due to the annually recurring "ozone hole," stable meteorological conditions, frequent cloudless days, constant high surface albedo, negligible aerosol influence, and virtually no diurnal change of the solar zenith angle (SZA). The conditions at BRW are quite different. Cloud cover is highly variable during fall, and significant changes in surface albedo occur because of springtime snowmelt and changes in sea ice coverage.

In 2002 and 2003 a new data version (Version 2) was prepared for the entire SPO UV data set. Compared to the currently published version (Version 0), the Version 2 data set is of higher accuracy and features a larger number of data products. Version 2 spectra are corrected for the cosine error [*Bernhard et al*., 2003b] and are provided on a uniform wavelength grid. New data products include dose rates for additional action spectra (such as erythema), spectra calculated with a radiative transfer model for referential purposes, total column ozone, and cloud optical depth.

As an example of network UV data, Figure 1 presents time-series of daily doses for two data products, the integral of spectral irradiance between 342.5 and 347.5 nm (top panel of Figure 1), and erythemal (sunburn action spectrum from the work of *McKinlay and Diffey* [1987]) daily dose (bottom panel). The 342.5–347.5 nm integral is not affected by atmospheric ozone absorption; variability beyond the annual cycle is mostly caused by differences in cloud cover. There is little variation in the SPO data set since clouds at the South Pole are relatively infrequent, optically thin, and their impact on UV is further mitigated by high albedo [*Nichol et al*., 2003]. In contrast, BRW data show a comparatively large variability in the fall when albedo is low and clouds are more frequent. Summer daily doses at SPO are generally higher than at BRW. At the South Pole, instantaneous values from all times of the day contribute almost equally to the daily dose because of the small diurnal variation of SZA. Even though noontime values at BRW are higher, low radiation levels from the "midnight sun" reduce daily doses below SPO levels.

Erythemal daily doses are affected by atmospheric ozone concentrations and, consequently, exhibit a large increase at SPO whenever the ozone hole is above the station. Depth and duration of ozone depletion are highly variable from year to year, leading to large interannual changes in erythemal UV. For example, the highest erythemal daily dose observed at SPO was in late November 1998 at a time when total ozone values were low and when the Sun's elevation was only 1.5° below the summer

Table 1. Installation Sites

Site	Latitude	Longitude	Established	Location
South Pole	90°00'S	–	February 1988	ARO*
McMurdo Station	77°51'S	166°40'E	March 1988	Arrival Heights
Palmer Station	64°46'S	64°03'W	May 1988	T-5 Building
Ushuaia, Argentina	54°49'S	68°19'W	November 1988	CADIC†
Barrow, Alaska	71°18'N	156°47'W	December 1990	UIC‡
San Diego, California	32°45'N	117°11'W	October 1992	Biospherical Instruments Inc.

*ARO: Atmospheric Research Observatory, system relocated to this new, joint CMDL facility in January 1997.
†CADIC: Centro Austral de Investigaciones Cientificas, Argentina.
‡ UIC: Ukpeagvik Inupiat Corporation.

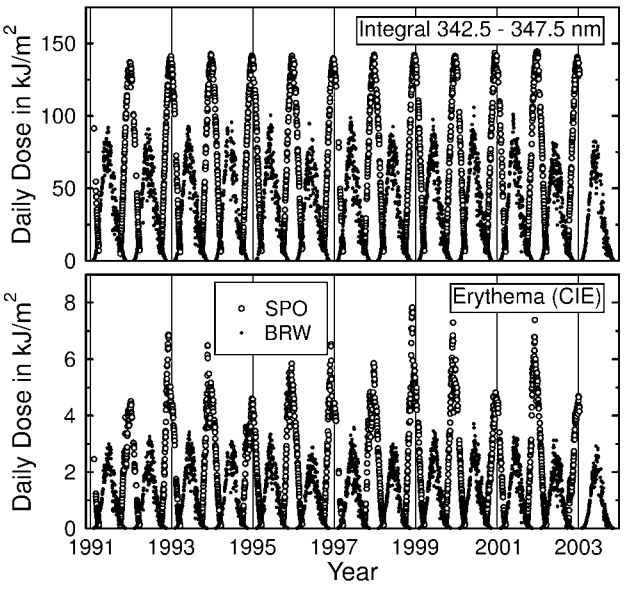

Figure 1. Daily dose of the integral of spectral irradiance between 342.5-347.5 nm (top panel) and erythemal daily dose (bottom panel) for SPO and BRW. SPO data are from the Version 2 data set; BRW data are from Version 0. BRW data from 2003 are preliminary and subject to revision.

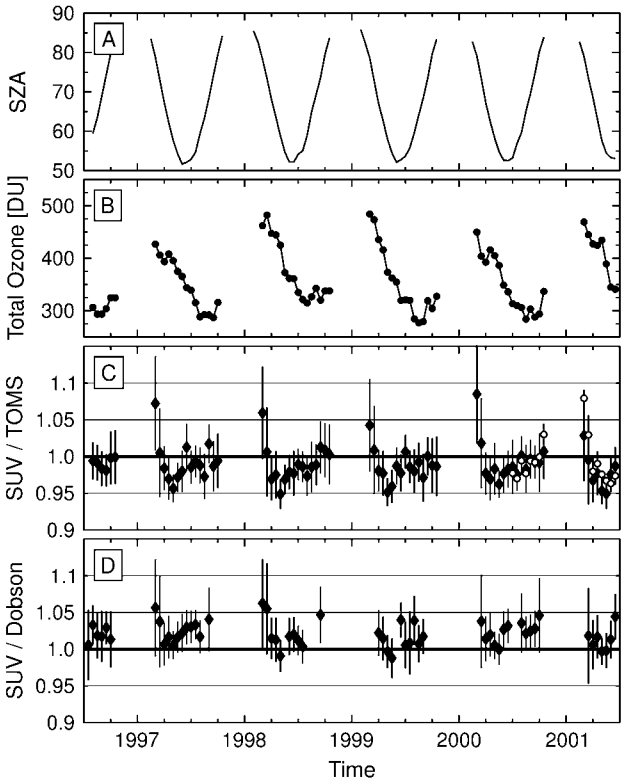

Figure 2. Comparison of bi-weekly averages of SUV-100, TOMS, and Dobson ozone measurements at BRW for 1996–2001. (A) Average solar zenith angle of the observations included. (B) Average total column ozone measured by SUV-100. (C) Ratio of total ozone values measured by SUV-100 and TOMS. Scan-mirror error corrected TOMS data are shown as black diamonds, uncorrected data as open circles. The error bars indicate the 2-σ uncertainty of the bi-weekly mean values. (D) Ratio of total ozone values measured by SUV-100 and CMDL Dobson.

solstice peak. In contrast, the early breakup of the ozone hole in 2002 led to comparatively low UV levels. Ozone depletion is less pronounced at BRW, and variability in erythemal dose is considerably smaller than at SPO.

TOTAL COLUMN OZONE AT BRW AND SPO

A new method was recently developed to derive total column ozone from global irradiance data [*Bernhard et al.*, 2003c]. For clear skies and SZA smaller than 75°, the 2-σ uncertainty of total ozone values calculated with this method varies between ±2 and ±3.5%. For SZAs larger than 75° the uncertainty increases because of the method's sensitivity to the vertical distribution of ozone in the atmosphere (the ozone profile). The influence of the ozone profile on calculated total ozone values is discussed in the work of *Bernhard et al.* [2003c] in detail.

Ozone values derived with the new method for BRW were compared with overpass data from National Aeronautics and Space Administration's (NASA) Earth Probe Total Ozone Mapping Spectrometer (TOMS) satellite and Dobson measurements performed by CMDL. Figure 2 shows the ratios SUV/TOMS and SUV/Dobson for 1996–2001. Ratios were averaged over 14-day periods to reduce random variations from cloud influence and to better illustrate the differences between the three data sets. For February–June, SUV-100 ozone data averaged 2.2% lower than TOMS and 1.8% higher than the Dobson measurements. For July–October, SUV-100 data are 0.9% lower than TOMS and 2.5% higher than the Dobson data.

The algorithm from the work of *Bernhard et al.* [2003c] was also used to calculate total column ozone from SUV-100 measurements at SPO. Ozone and temperature profiles were taken from CMDL balloon soundings. Figure 3 shows the ratio of the SUV-100 data set to collocated CMDL Dobson measurements as a function of SZA. Only the SUV-100 spectra measured within 90 minutes of the Dobson observations were used for the comparison. On average, the SUV-100 total ozone values are 2% higher than the Dobson values. The difference increases with the SZA: it is 1.2% at 67°, 3.1% at 80°, and 5.9% at 83° as the fit curve in Figure 3 indicates. Closer inspection revealed that some of the apparent SZA dependence may in fact be total ozone dependence. At the same SZA, deviations between the two data sets tend to be larger for the low ozone values measured in October and November during the ozone hole period than for the higher ozone values measured in February and March. When the comparison was restricted to Dobson "AD" measurements, the SZA-angle dependence disappeared. This indicates that a part of the discrepancy could be caused by a small bias between Dobson AD and CD observations, since only the latter observation mode is applied for large SZA. As of this writing, the data are still under evaluation, and the recently released TOMS Version 8 data set is expected to further improve our understanding of the observed discrepancies.

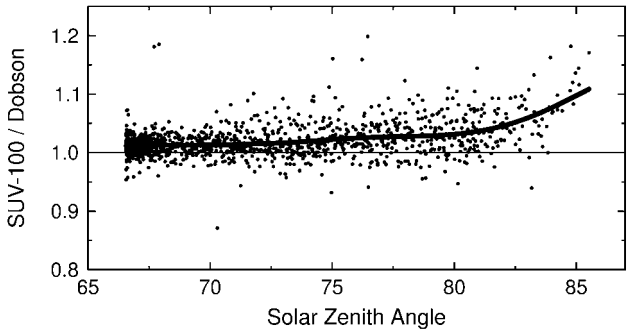

Figure 3. Ratio of SUV-100 and Dobson total column ozone measurements at SPO. Data is from 1991-2003. The thick line is a trend line to the data set.

Acknowledgments. The NSF/OPP UV Monitoring Network is operated by Biospherical Instruments Inc. under a contract from the NSF/OPP via Raytheon Polar Services Company (RPSC). The Ukpeagvik Inupiat Corporation provided assistance in the original installation at Barrow. We wish to express our gratitude to Dan Endres, Malcolm Gaylord, Glen McConville, Don Neff, and Daren Blythe from CMDL who operated the SUV-100 instrument at Barrow. Cordial thanks also go to numerous operators from Antarctic Support Associates (ASA) and RPSC for maintaining our instrument at SPO.

REFERENCES

Bernhard, G., C.R. Booth, J.C. Ehramjian, and V.V. Quang (2003a), *NSF Polar Programs UV Spectroradiometer Network 2000-2001 Operations Report*, Biospherical Instruments Inc., San Diego, CA.

Bernhard, G., C.R. Booth, J.C. Ehramjian (2003b), The quality of data from the National Science Foundation's UV Monitoring Network for Polar Regions, in *Ultraviolet Ground- and Space-based Measurements, Models, and Effects II*, edited by W. Gao, J.R. Herman, G. Shi, K. Shibasaki, and J.R. Slusser, *Procceedings of SPIE Int. Soc. Opt. Eng.*, *4896*, pp. 79-93.

Bernhard, G., C.R. Booth, and R.D. McPeters (2003c), Calculation of total column ozone from global UV spectra at high latitudes, *J. Geophys. Res*., *108*(D17), 4532, doi:10.1029/2003JD003450.

Booth, C.R., T.B. Lucas, J.H. Morrow, C.S. Weiler, and P.A. Penhale (1994), The United States National Science Foundation's polar network for monitoring ultraviolet radiation, in *Ultraviolet Radiation in Antarctica: Measurement and Biological Effects*, edited by C.S. Weiler and P.A. Penhale, *Antarct. Res. Ser.*, *62*, pp. 17-37, Am. Geophys. Union, Washington D.C.

McKinlay, A.F. and B.L. Diffey (1987), A reference action spectrum for ultraviolet induced erythema in human skin, in *Commission International de l'Éclairage (CIE), Research Note*, *6*(1), 17-22.

Nichol, S.E., G. Pfister, G.E. Bodeker, R.L. McKenzie, S.W. Wood, and G. Bernhard (2003), Moderation of cloud reduction of UV in the Antarctic due to high surface albedo, *J. Appl. Meteorol.*, *42*(8), 1174–1183.

Global Positioning System Measurements of Water Vapor, Barrow, Alaska

J. T. FREYMUELLER
Geophysical Institute, University of Alaska, Fairbanks, 99775

INTRODUCTION

The Global Positioning System (GPS) is becoming a widely used tool for the estimation of atmospheric water vapor. A ground-based GPS receiver can measure its position daily, as well as hourly or more frequent atmospheric path (zenith) delays. The University of Alaska, Fairbanks (UAF) Geophysical Institute installed a GPS receiver at the CMDL facility in Barrow, Alaska, in May 2002 to provide real-time and post-processed atmospheric delay measurements as part of the University Corporation for Atmospheric Research (UCAR) SuomiNet project. This site was given the site code SG27 by SuomiNet personnel. Our analysis of these data is focused on retrospective and long-term analysis of atmospheric variations rather than immediate forecasting. However, precision and accuracy determined from such a long-term study is a key ingredient in understanding how to use more rapid analyses for forecasting or assimilation in weather models.

This report describes the site installation, the initial results obtained so far, and the expected improvements to come. In addition to our analysis, data from this site are analyzed in real time by UCAR as part of SuomiNet, and the results of the analysis are available at their Web page (http://www.suominet.ucar.edu/). Raw data from SG27 is available from UCAR and from UNAVCO, Inc. (http://www.unavco.org/).

SITE INSTALLATION

The GPS site SG27 was installed on 3 May 2002 by the Geophysical Institute with assistance from personnel at the University NAVSTAR Consortium (UNAVCO, Inc.). The instrumentation consists of a Trimble 4700 GPS receiver with a Trimble micro-centered antenna, a Paroscientific, Inc. MET-3 meteorological package (temperature, pressure, humidity), and a PC to log the data and stream it over the Internet to UCAR in Boulder, Colorado. All GPS equipment was tested and configured at the UNAVCO, Inc. Boulder facility prior to shipping it to Barrow.

The GPS antenna is mounted on a leveling mount attached to the top of a wooden piling. The piling is frozen into a hole drilled into the frozen ground, a standard practice in Barrow for mounting instruments. The piling is set away from the CMDL observatory building and other instruments to provide a clear sky view and to minimize possible interference. The Paroscientific meteorological package was mounted to the same piling below the GPS receiver. Cables were run through a conduit into the main CMDL building to the PC. The PC is connected to the Internet and streams data to UCAR in Boulder. UCAR carries out real-time processing and makes the data available in 24-hour data files via UNAVCO, Inc.

Operation over the last 1.5 years has gone smoothly. Real-time data flow has been continuous except for occasional interruptions to the Internet service when the entire CMDL facility is offline; these interruptions have lasted as long as a few days. This interruption of service affects UCAR's real-time analysis, but it does not impact the 24-hour data files available from UNAVCO, Inc. that are used in our analysis.

INITIAL RESULTS

The goal, for a post-processed analysis of these data, is to provide the highest-accuracy tropospheric estimates for long-term studies rather than immediate estimates for forecasting purposes. To achieve this, we analyze the GPS data from SG27 in a network mode with sites from around Alaska. We fix the GPS satellite orbits, estimate daily site coordinates, zenith tropospheric delays, and a variety of nuisance parameters. Site coordinates are unconstrained and, after estimation, are transformed into the International Terrestrial Reference Frame, version 97 (ITRF97). The model includes an a priori estimate of the "dry" tropospheric delay (air mass) based on the site elevation and latitude. This removes about 80% of the tropospheric path delay, and the remaining path delay is dominated by the "wet" component (water vapor). The remaining path delay is estimated using a single zenith tropospheric delay along with a standard elevation mapping function and a daily azimuthal gradient. The zenith delay is estimated as a random walk process producing an estimate of the path delay every 5 minutes.

Site coordinates are not of immediate interest to the atmospheric community, but they are very sensitive indicators of any errors or mismodeling in a GPS solution. Such errors are not so easily seen in tropospheric delay time series. The coordinate time series for SG27 is shown in Figure 1. A few outliers in the time series result from poor quality solutions that are being addressed. The scatter of the solutions is acceptable if the outliers are excluded.

Three notable features can be seen in the time series. The first is a series of deviations from the linear trend in the latitude component shortly after 2002.5. The cause of these deviations is not clear yet. The second is a jump in the longitude component at about 2002.8, just a couple of weeks before the 2002 Denali Fault earthquake (3 November 2002, shown by the dashed line at 2002.841 in Figure 1). This jump resulted from an error in the realization of the reference frame caused by an offset in the position of one of the sites used to define the reference frame transformation. Because it is purely a reference frame error, it has no impact on the tropospheric delay estimates. The final notable feature is a clear periodic noise signal apparent in the height component with a period of a few weeks. Our present hypothesis is that this results from unmodeled ocean tidal loading. If that hypothesis is correct, then the loading error would also produce a similar periodic error in the tropospheric delay. Any mismodeling that impacts the height coordinate also affects the tropospheric delay estimates.

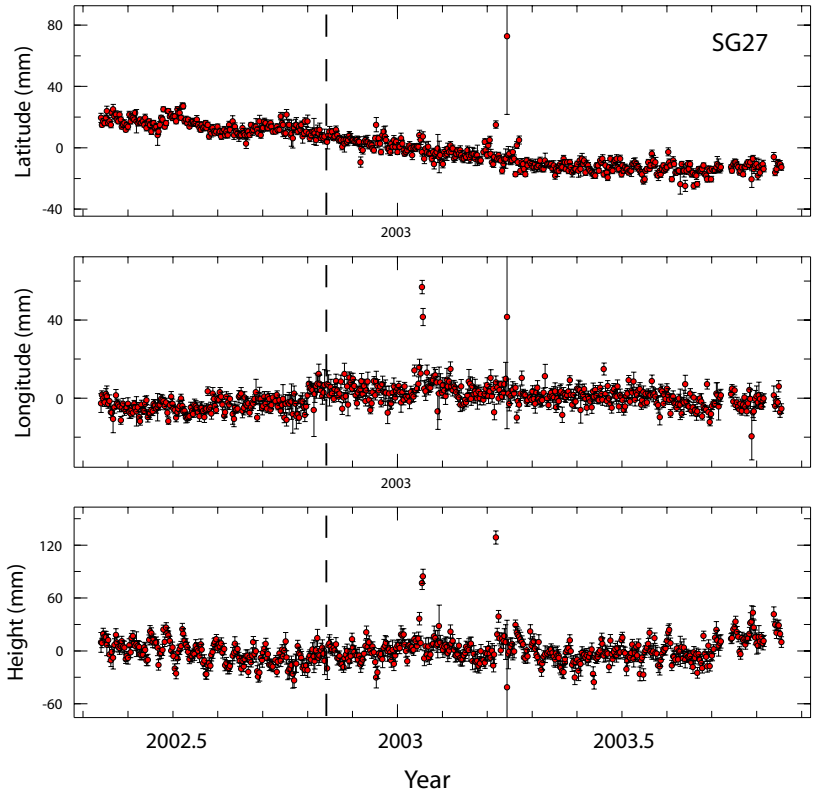

Figure 1. Coordinate time series from the GPS site SG27 at the CMDL facility in Barrow. The vertical dashed line indicates the time of the 2002 M_W 7.9 Denali Fault earthquake on 3 November 2002. The offset in the time series that precedes the earthquake results from a recently identified reference frame error. The tic marks represent 36.525 days, therefore, 2002.5 represents 1 July 2002.

The time series of total tropospheric zenith path delays is shown in Figure 2. The total path delay is a sum of the path delay due to air mass (dry delay) and water vapor (wet delay). The total range of variation over the course of 2 years is quite small with almost all estimates falling within a range of only 15 cm. Some features are clear with high-frequency variations primarily concentrated in the summer months, presumably reflecting variability in water vapor. Variations in the winter are dominated by long-period variations in atmospheric pressure. Since these results were obtained only quite recently, we have not yet begun to explore them in full.

Expected Improvements

We anticipate some significant improvements in our solutions within the next few months, and at least one of these should have a strong impact on the accuracy of the tropospheric delay estimates. We plan to reanalyze our complete solution set over the next few months. The main improvement should come from the modeling of the ocean tidal loading signal, although detailed model improvements may also make a difference for some sites. We will evaluate the impact of the new solution series on the tropospheric delay estimates. We will then make a rigorous comparison of the GPS delay estimates along with those that would be inferred from independent measurements collected by CMDL.

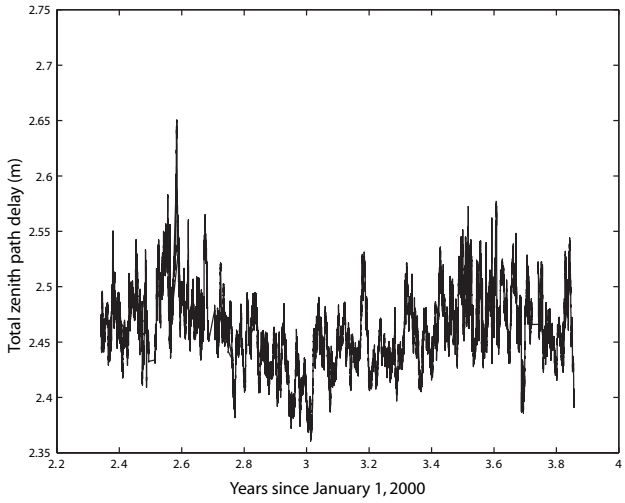

Figure 2. Time series of total zenith tropospheric delay at SG27.

Acknowledgments. This instrument was installed as part of the University of Alaska's cooperation in the SuomiNet project (http://www.suominet.ucar.edu/) coordinated by UCAR. Site installation was supported by the UNAVCO, Inc. Boulder facility, then a part of UCAR. We thank Bjorn Johns and Shad O'Neel for their assistance with the installation.

Microclimate Data from an Evapotranspiration Station at Cape Matatula, Tutuila, American Samoa

SCOT K. IZUKA
U.S. Geological Survey, Honolulu, Hawaii 96813

THOMAS W. GIAMBELLUCA AND MICHAEL A. NULLET
Department of Geography, University of Hawaii, Honolulu, Hawaii 96822

FA'AMAO O'BRIEN ASALELE, JR.
American Samoa Environmental Protection Agency, Pago Pago, American Samoa 96799

INTRODUCTION

The need to assess, manage, and protect ground-water resources on Tutuila, American Samoa, has become increasingly important as ground-water development has grown from a few dug wells and scattered spring catchments prior to the 1960s, to more than a hundred drilled wells by the end of the 20th century [*Davis*, 1963; *Bentley*, 1975; *Izuka*, 1999]. Quantitative assessment of the rate of ground-water recharge on Tutuila, however, requires reliable estimates of several hydrologic parameters, including the loss of water from the land surface by evapotranspiration (ET). In an effort to estimate island-wide ET on Tutuila, the U.S. Geological Survey, in cooperation with the American Samoa Environmental Protection Agency, is operating a network of ET stations to monitor the microclimate at several locations on Tutuila (Figure 1). The microclimate data will be used in an energy-balance equation developed by *Penman* [1948] to estimate potential ET.

This report summarizes the microclimate data collected at the ET station deployed on the grounds of the American Samoa CMDL observatory (SMO) at Cape Matatula from 3 May 2001 to 4 June 2002. The site was selected because it offered (1) the opportunity to gather data near the easternmost point of Tutuila, (2) access to long-term climatic data collected at the observatory, and (3) logistic advantages such as easy access, an unobstructed outdoor area, and security.

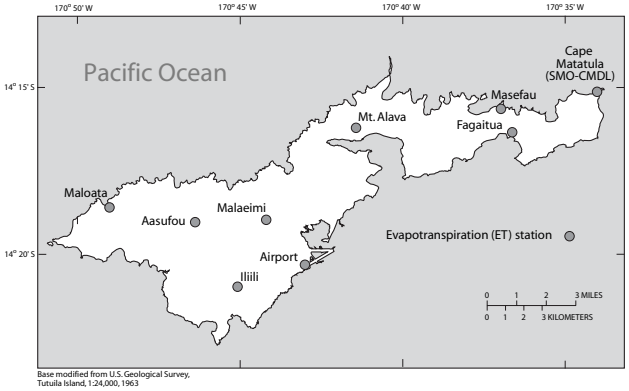

Figure 1. Locations of evapotranspiration stations deployed for this study on Tutila, American Samoa.

INSTRUMENTATION, DATA COLLECTION AND PROCESSING

The ET station consisted of above-ground and subsurface sensors that monitored net radiation, relative humidity, air and soil temperature, soil heat flux, soil moisture, wind speed, and rainfall (Table 1, Figure 2). All sensors were placed within 2.3 m of the ground surface. An automatic data logger controlled the

Table 1. Parameters Monitored at the Microclimate Station, Cape Matatula, Tutuila, American Samoa

Parameter	Height of Sensor, Relative to Ground Surface (m)	Frequency of Measurements and Type of Data Stored
Net radiation	1.91	Hourly average of measurements made every 10 seconds
Wind speed	2.18	Hourly average of measurements made every 10 seconds
Relative humidity	2.21	Hourly average of measurements made every 10 seconds
Air temperature	2.21	Hourly average of measurements made every 10 seconds
Rainfall	2.13	Minute totals and hour totals
Soil moisture	0.00 to –0.30	One reading every hour
Soil heat flux*	–0.08	Hourly average of measurements made every 10 seconds
Average soil temperature†	–0.02 and –0.06	Hourly average of measurements made every 10 seconds

*Average of two sensors measuring soil heat flux at two locations
†Average of four thermocouples buried at two depths for two locations

Figure 2. Evapotranspiration station at the SMO Observatory on Tutuila, American Samoa.

sensors, made simple computations, and stored data. For most sensors, the logger took measurements every 10 seconds. Every hour on the hour, the logger computed and stored an average of the 10-second measurements made over the preceding hour. Exceptions to this procedure were the measurements for soil moisture and rainfall. The logger took measurements from the soil-moisture probe once every hour. To measure rainfall, a tipping-bucket gage was used where each tip represented 0.254 mm of rain. The data logger converted the tip counts to rainfall and summed the total rainfall for each minute as well as for each hour. A 12-volt battery and a 10-watt solar panel provided power to the station. The station was visited about every 2 weeks for routine maintenance and to retrieve data. The data were screened to eliminate any spurious values that may have resulted from calibration drift or instrument failure.

RESULTS

Except for relative humidity, the hourly microclimate data from the ET station at SMO is essentially continuous for the entire period of deployment. Calibration of the relative humidity sensor began to drift on 2 October 2001. Because the drift was gradual, it was not discovered until after the station was dismantled in June 2002, and the data from the relative-humidity sensor were compared with relative humidity computed from concurrent air and dew point temperatures measured at SMO (ftp://140.172.192.211/met/hourlymet/smo, downloaded on 14 August 2003). Therefore, all relative-humidity data from 2 October 2001 through the end of the monitoring period at this site were omitted from this summary.

The hourly data from the ET station covers the period from 1100 on 3 May 2001 through 1100 on 4 June 2002 and are summarized in graphs and tables of daily and monthly means (except rainfall, for which totals are shown) in Figures 3 and 4. For all data, except relative humidity, the period of record for the daily values begins on the first complete day of data, 4 May 2001 and extends through the last complete day of data, 3 June 2002; the period of record for the monthly values extends from the first complete month of data, June 2001 through the last complete month of data, May 2002. Because of the drift in the calibration of the relative humidity sensor, the period of record for daily values extends from 4 May through 1 October 2001, and the period of record for monthly values extends from June 2001 through September 2001. Maximum, minimum, and average daily and monthly values are given in Tables 2 and 3.

Table 2. Maximum, Minimum, and Mean Daily Microclimate Values from the Evapotranspiration Station at Cape Matatula, Tutuila, American Samoa, for 4 May 2001 through 3 June 2002

	Maximum		Minimum		
Parameter	Value	Date	Value	Date	Mean
Daily mean net radiation (W m^{-2})*	198.39	28 October 2001	-3.46	4 June 2001	120.03
Daily mean soil heat flux (W m^{-2})*	9.45	11 December 2001	-12.04	20 March 2002	0.20
Daily mean soil temperature (^{o}C)	37.92	5 February 2002	28.85	28 July 2001	33.73
Daily mean air temperature (^{o}C)	30.32	6 February 2002	20.92	6 December 2001	27.39
Daily mean relative humidity (%)†	92.58	21 September, 2001	42.54	19 May 2001	78.49
Daily mean wind speed (m s^{-1})	3.90	30 December 2001	0.00	27April 2002	0.95
Daily mean soil moisture (%)‡	43.76	10 June 2001	14.76	20 September 2001	29.65
Daily rainfall (mm)	105.67	26 December 2001	0.00	Several dates	6.70

*Positive values indicate net flow of energy is downward
†Period of record is 4 May 2001 through 2 October 2001
‡Percent by volume

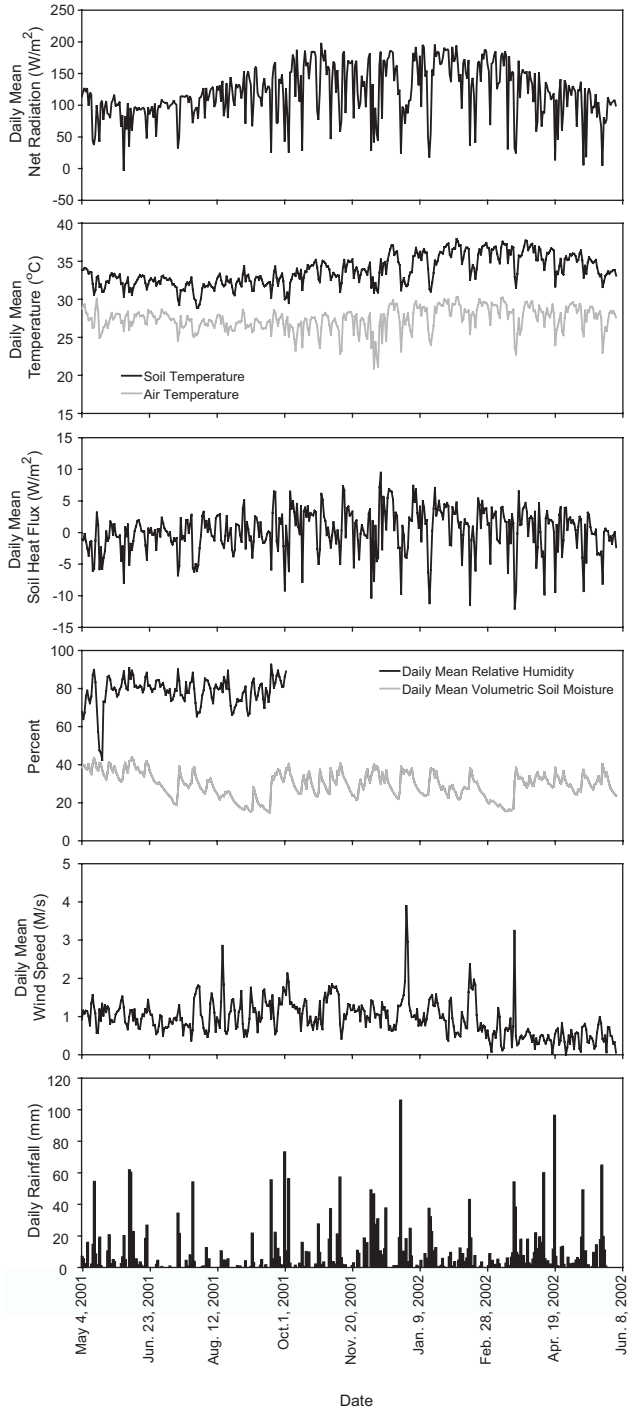

Figure 3. Daily microclimate at the evapotranspiration station at Cape Matatula, Tutuila, American Samoa, 4 May 2001 through 3 June 2002.

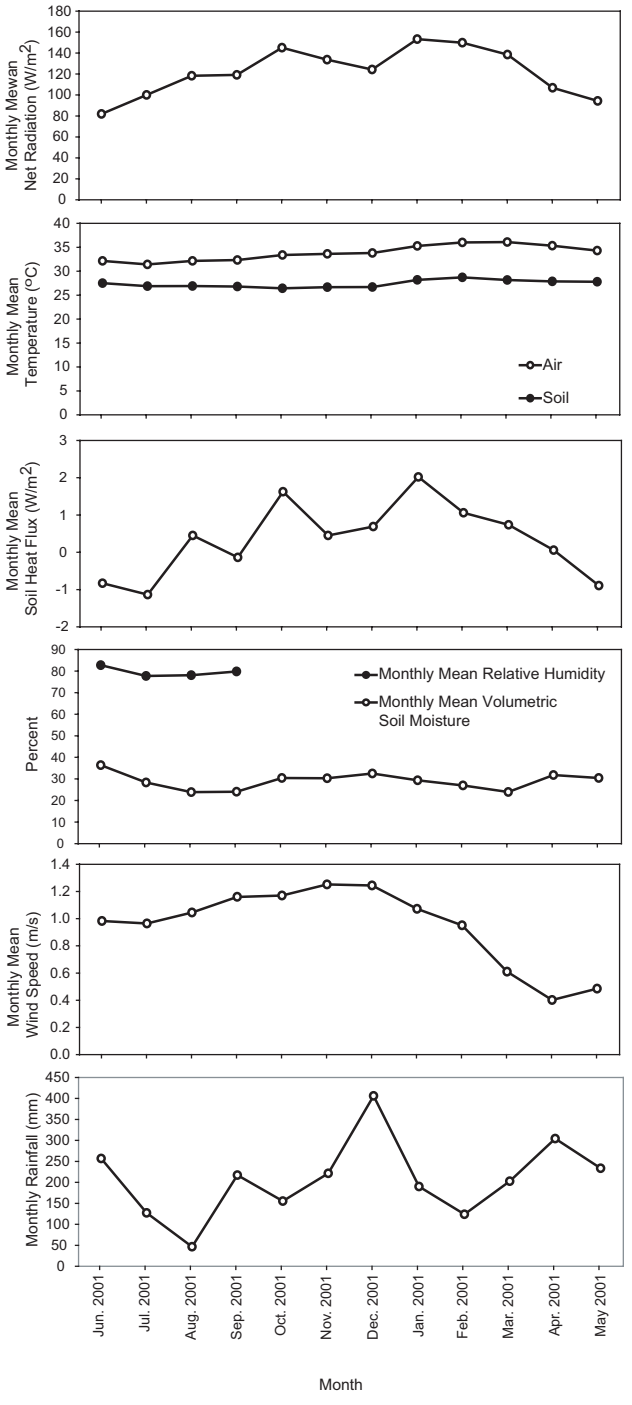

Figure 4. Monthly microclimate at the evapotranspiration station at Cape Matatula, Tutuila, American Samoa, June 2001 through May 2002.

Table 3. Maximum, Minimum, and Mean Monthly Microclimate Values from the Evapotranspiration Station at Cape Matatula, Tutuila, American Samoa, for June 2001 through May 2002

	Maximum		Minimum		
Parameter	Value	Month	Value	Month	Mean
Monthly mean net radiation (W m^{-2})*	153.31	January 2002	81.92	June 2001	122.13
Monthly mean soil heat flux (W m^{-2})*	2.02	January 2002	-1.13	July 2001	0.34
Monthly mean soil temperature (^{o}C)	36.08	March 2002	31.43	July 2001	33.82
Monthly mean air temperature (^{o}C)	28.72	February 2002	26.44	October 2001	27.39
Monthly mean relative humidity (%)†	82.74	June 2001	77.70	July 2001	79.59
Monthly mean wind speed (m s^{-1})	1.25	November 2001	0.40	April 2002	0.95
Monthly mean soil moisture (%)‡	36.42	June 2001	23.88	August 2001	29.04
Monthly rainfall (mm)	406.15	December 2001	46.48	August 2001	207.18

*Positive values indicate net flow of energy is downward
†Period of record is June through September 2001
‡Percent by volume

REFERENCES

Bentley, C.B. (1975), Ground-water resources of American Samoa with emphasis on the Tafuna-Leone Plain, Tutuila Island, *U.S. Geol. Surv. Water-Res. Invest. Rep*., pp. 29-75.

Davis, D.A. (1963), Ground-water reconnaissance of American Samoa, *U.S. Geol. Surv. Water-Supply Pap*., 1608-C, 21 pp.

Izuka, S.K. (1999), Hydrogeologic interpretations from available ground-water data, Tutuila, American Samoa, *U.S. Geol. Surv. Water-Res. Invest. Rep., 99-4064*, 2 sheets.

Penman, H.L. (1948), Natural evaporation from open water, bare soil, and grass, *Procceedings of the Royal Soc. London,* A193, pp. 120-146.

Rossby Wave Breaking over Mauna Loa Observatory, Hawaii, During Summer 2002

THIERRY LEBLANC AND I. STUART MCDERMID
Table Mountain Facility, Jet Propulsion Laboratory, California Institute of Technology, Wrightwood, 92397

ALAIN HAUCHECORNE
Service d'Aéronomie du CNRS, BP3, 91371 Verrières-le-Buisson cedex, France

INTRODUCTION

In the framework of the international Network for the Detection of Stratospheric Change (NDSC), the Jet Propulsion Laboratory (JPL) developed a differential absorption ozone lidar system for long-term stratospheric measurements at Mauna Loa Observatory (MLO), Hawaii (19.5ºN). The MLO location is a strongly active Stratosphere-Troposphere Exchange (STE) region due to the particular configuration of the circulation over the Pacific Ocean at the exit of the Asian monsoon upper circulation. Using maps of isentropic Ertel's potential vorticity (IPV), *Hoskins* [1991] pointed out that significant stratosphere-to-troposphere transport occurs at 360 K in the eastern side of the subtropical anticyclone associated with the Asian summer monsoon. *Chen* [1995] suggested the presence of a subtropical surf-zone where Rossby wave breaking (RWB) occurs preferentially near the subtropical tropopause. These RWB events are materialized on isentropic maps of Ertel's potential vorticity (PV) by the irreversible deformation of the PV contours due to the reversal of the meridional PV gradient. These deformations produce large positive PV anomalies during what is commonly called "equatorward breaking." Such an event occurred in July 2002 over Hawaii and will be outlined here. Its impact on ozone as measured by the MLO lidar will be shown.

DATASETS AND METHODOLOGY

The JPL lidar at MLO [*McDermid et al.*, 1990] typically operates 2 hours per night, 4 to 5 nights a week (since 1993). The results are archived on a monthly basis in the NDSC database (http://www.ndsc.ws). The data set used here extends from 1 June to 30 September 2002 and results in 55 ozone profiles (12-55 km) with a 300-m vertical resolution. The ozone number density was converted into mixing ratio, then interpolated vertically onto 55 isentropic levels (300 to 2000 K, every 5 K near the tropopause) using global 6-hour interval analyzed winds, temperature, and geopotential height from the European Centre for Medium-Range Weather Forecasts (ECMWF) [*Simmons and Hollingsworth*, 2002 and references therein]. IPV calculated from the ECMWF was input to the high-resolution (3-points per degree) IPV-advection model Modele Isentrope du transport Meso-echelle de l'Ozone Stratospherique par Advection (MIMOSA) [*Hauchecorne et al.*, 2002]. In an idealized adiabatic, frictionless atmosphere, IPV is advected by the winds as if it were a passive chemical tracer. Because of the variation with height of the latitudinal gradient of ozone, a positive correlation with PV in the lower stratosphere is expected. After a 15-day spin-up period during which filamentary structures develop to full scale, the high-resolution IPV outputs from MIMOSA were compared to the ozone mixing ratios measured by the MLO lidar.

OZONE-PV RELATIONSHIP ABOVE MLO NEAR THE TROPOPAUSE

Figure 1 shows (a) the deseasonalized modified (i.e., multiplied by $(\theta/\theta_0)^{-9/2}$, with θ_0 = 350 K [*Lait*, 1994]) IPV time-height cross section in the tropopause region output from MIMOSA through the summer of 2002, and (b) the corresponding time-height cross section of the deseasonalized ozone mixing ratio measured by lidar. The time series at each altitude were deseasonalized by applying a least-square 2nd degree polynomial fit to the 4-month series and then calculating the deviations from this fit. The approximate vertical locations of the World Meteorological Organization (WMO), in black, and the dynamical, in purple, tropopauses calculated from the coarse grid data are superimposed. The WMO tropopause is based on the vertical position and persistence of a threshold temperature lapse rate [*WMO*, 1957]. The dynamical tropopause was chosen here to be the isentropic level at which the vertical gradient of IPV maximizes in a layer situated between the midtroposphere and the midstratosphere.

Around the tropopause (350-380 K), high variability on timescales of a few days can be observed during the first part of the summer. This is the common signature of Rossby wave fluctuations and other synoptic disturbances. The positive correlation between PV and the ozone mixing ratio is clearly observed. The maximum variability observed between the 350 and 370 K levels is typified by alternative periods of tropospheric and stratospheric regimes at a given isentropic level. The positive anomalies correspond to the passing of lower stratospheric midlatitude air masses when the tropopause in the North Pacific region is meridionally displaced southward of Hawaii by Rossby waves. The negative anomalies correspond to periods of upper tropospheric tropical regimes when the tropopause in the tropical Pacific region is meridionally displaced northward of Hawaii. The stratospheric episode of 13 July 2002 is now outlined.

CASE STUDY OF A ROSSBY WAVE BREAKING EVENT OVER MLO

Around 12-14 July 2002 the ozone mixing ratio anomaly measured by lidar near the tropopause exceeded 100% (Figure 1b). The evolution of the IPV field output from MIMOSA on the 350 K surface between 9 and 16 July 2002 is depicted in Figures 2a through 2f. The IPV is plotted with color contours, and the horizontal wind speed is superimposed with white contour lines. Until 12 July 2002 the MLO lidar sampled air parcels located in the vicinity of the subtropical jet far south of the region where the tropopause intersects that isentrope. The air sampled at this altitude was of tropical upper tropospheric origin, characterized

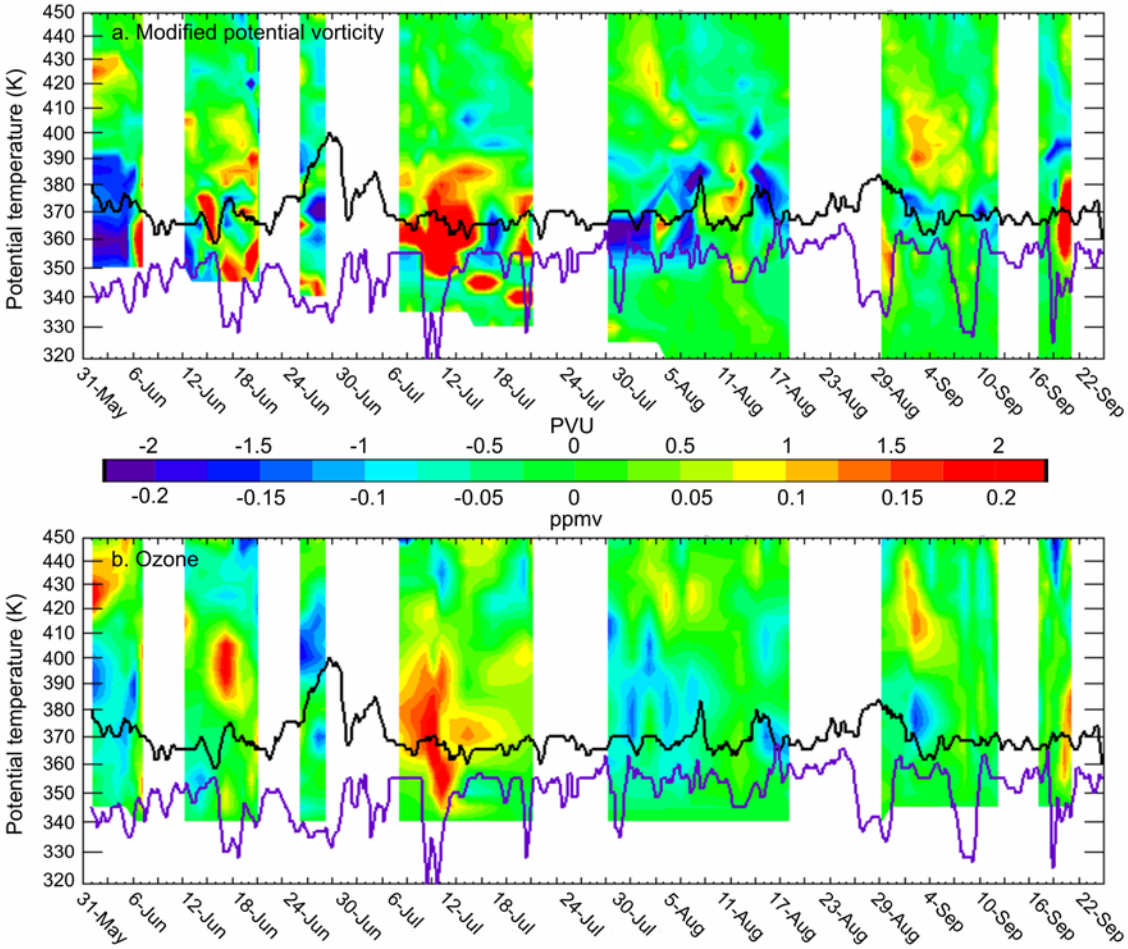

Figure 1. Altitude-time cross sections of deseasonalized MPV computed from ECMWF/MIMOSA above MLO (a), and deseasonalized ozone mixing ratio measured by the MLO lidar (b).

by low ozone mixing ratio, low IPV, and a high tropopause (not shown). By 13 July 2002, following strong deformation by Rossby waves, an upper trough formed in the North Central Pacific and slid southwards to the Hawaiian Islands, rolling up clockwise around a high-pressure cell located northwest of Hawaii. On 12 July 2002 at this level, the MLO lidar sampled lower stratospheric air (high ozone values, high IPV, and a lower tropopause). This air was transported southward from the Aleutian region by the tropopause jet tilting along the western edge of this extended trough. On this date, the subtropical jet shifted south of the Hawaiian Islands, and the elongation of the trough eventually led to the development of a cutoff system that formed over Hawaii and was later advected eastward following the mean zonal flow. The cutoff system, initially circular, quickly became elongated as seen in Figure 2f. After the passing of the cut-off system over the island (16 July 2002), the lidar again sampled upper tropospheric tropical air with similar characteristics as those described for 9 July 2002. The evolution of this particular RWB event is typical and follows the behavior of the LC1-type RWB event modeled in the work of *Thorncroft et al*. [1993] remarkably well, including the upstream tilting of the high PV tongue and the elongated shape of the newly formed cut-off. This cut-off system never reconnected with the main high PV reservoir, most likely implying net isentropic transport and mixing of high-latitude lower-stratospheric air into the subtropical upper troposphere.

Conclusion

There is a significant positive correlation between ozone that was locally measured by lidar over Mauna Loa Observatory and the potential vorticity from ECMWF observed during the summer of 2002 near the tropopause. The signature of Rossby wave breaking events was easily identified as high PV intrusions over the Hawaiian Islands associated with the high values of ozone measured by lidar. The event of 13 July 2002 was outlined showing a typical LC1 type of breaking event [*Thorncroft et al*. 1993]. The next step is to extend the current study to all years and all seasons available since the MLO lidar began operating in order to isolate the STE and meridional transport signatures of

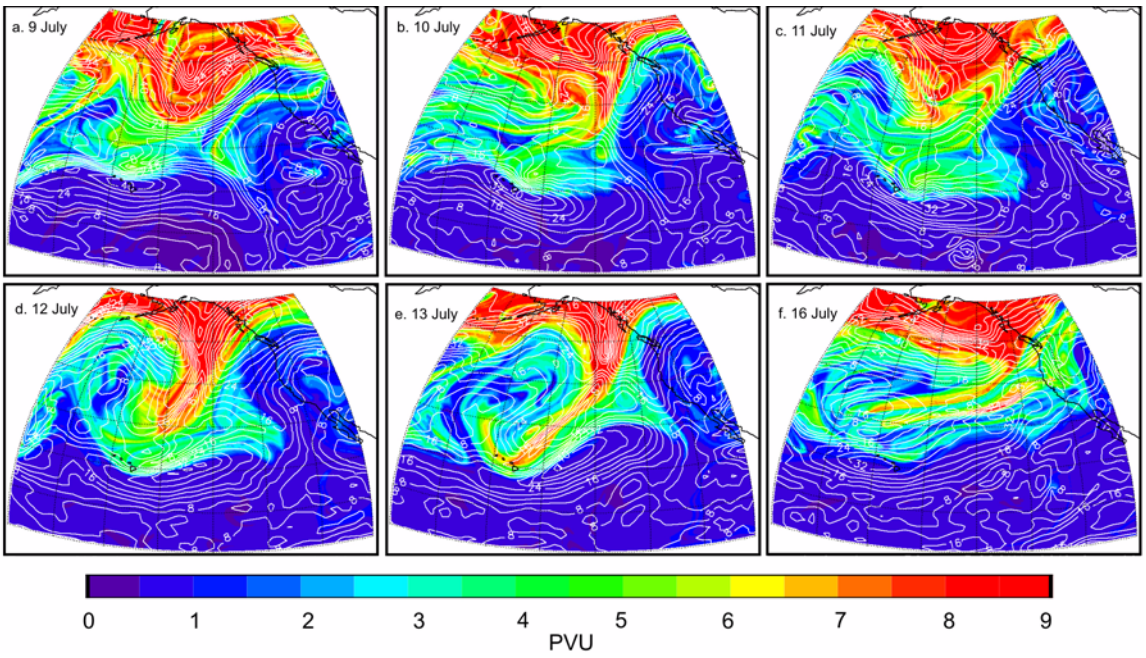

Figure 2. Isentropic maps of IPV output from MIMOSA IPV at 350 K on 9 (a), 10 (b), 11 (c), 12 (d), 13 (e), and 16 July 2002. The wind speed (in ms^{-1}) is superimposed with white contour lines.

many processes such as the El Niño/Southern Oscillation (ENSO) and the quasi-biennial oscillation (QBO). We expect eventually to relate most aspects of the lidar-observed ozone variability at MLO to the lower and midstratospheric circulation over the central and eastern Pacific.

Acknowledgments. The work described in this paper was carried out at the Jet Propulsion Laboratory, California Institute of Technology, under an agreement with the National Aeronautics and Space Administration. The authors would like to thank those other members of the JPL Lidar Team, D. A. Haner, J. Howe, and T. D. Walsh, who assisted in the collection of the data used here. The ECMWF data were made available for NDSC participants at the Norwegian Institute for Air Research (NILU), Norway.

REFERENCES

Chen, P. (1995), Isentropic cross-tropopause mass-exchange in the extratropics, *J. Geophys. Res*., *100*(D8), 16,661-16,674.

Hauchecorne, A., S. Godin, B. Heese, M. Marchand, and C. Souprayen (2002), Quantification of the transport of chemical constituents from the polar vortex to midlatitudes in the lower stratosphere using the high-resolution advection model MIMOSA and effective diffusivity, *J. Geophys. Res*., *107*(D20), 8289, doi: 10.1029/2001JD000491.

Hoskins, B.J. (1991), Towards a PV-θ view of the general circulation, *Tellus*, *43*, 27-35.

Lait, L.R. (1994), An alternative form for potential vorticity, *J. Atmos. Sci*., *51*, 1754-1759.

McDermid, I.S., S. Godin, and L. O. Lindquist (1990), Ground-based laser DIAL system for long-term measurements of stratospheric ozone, *Appl. Opt*., *29*, 3603-3612.

Simmons, A.J., and A. Hollingsworth (2002), Some aspects of the improvement in skill of numerical weather prediction, *Q. J. R. Meteorol. Soc*., *128*, 647-677.

Thorncroft, C.D., B.J. Hoskins , and M.F. McIntyre (1993), Two paradigms of baroclinic-wave life-cycle behavior, *Q. J. R. Meteorol. Soc*., *119*, 17-55.

WMO (World Meteorological Organization) (1957), Definition of the tropopause, *WMO Bull*., *6*, 136 pp., Geneva.

Artificial Windshielding of Precipitation Gauges in the Arctic

RICHARD J. MCCLURE
Natural Resources Conservation Service, Anchorage, Alaska 99501

INTRODUCTION

Precipitation gauges can provide good measurements for the water equivalent of snow precipitation provided the gauge is protected or shielded from wind effects. Unfortunately, there are no standards for collecting snow precipitation. Gauges located in exposed and windy areas may be totally unshielded, partially shielded by one or more buildings, or equipped with one of several types of artificial shields. The various shielding options in common use, therefore, produce a wide range of gauge catch efficiency. Also, the various studies of artificial shields in the United States and Canada have produced a wide range of results. This, in part, is due to the wide range of weather conditions under which the various studies were conducted. A lingering problem is applying the results to the local conditions of Alaska's tundra regions.

METHODS

A study of the windshield alternatives, under the unique conditions of Alaska's Arctic coastal region, was set up at the CMDL facility at Barrow during September 1989. Snowfall catches from four installed precipitation storage gauges were compared with that from an existing storage gauge protected by a Wyoming shield [*Hanson*, 1988]. Two of the new gauges were shielded, one with a Nipher shield [*Goodison et al*., 1983], the other with an Alter shield [*Alter*, 1937], and two were unshielded. One of the unshielded gauges was serviced on an event basis, the same as the three shielded gauges. The other unshielded gauge was treated as if it were a remote gauge, allowing rime to build up and dissipate naturally to see what effects rime had on the overall catch. The four installed gauges are 20.3-cm in diameter × 100-cm tall, mounted with the orifice 2-m above the normal ground surface. The existing Wyoming shield gauge is 30.5-cm in diameter × 2-m tall and is equipped with a Leupold-Stevens water-level recorder. In July 1993, wind storms blew over the Wyoming wind shield because the anchors were melted out in the permafrost. The storm was an unusual wind event for that time of year. The gauge was not rebuilt.

RESULTS

A comparison of the four gauges using ten winter seasons of total precipitation is shown in Table 1. The results confirm the catch of the Alter shield is 37 to 68% of the Nipher shield while the unshielded gauges range from 10 to 40% of the Nipher shielded precipitation gauge.

Table 1. Comparison of Total Precipitation of the Four Remaining Gauges

Dates	Nipher	Alter	Unshielded Serviced	Unshielded Unserviced
1993-1994 (5 Oct. 1993- 1 June 1994)	76.2 mm	38.1 mm	No record	23.9 mm
Percent of Nipher		50%		31%
1994-1995 (1 Oct. 1994-June 1,1995)	104.6 mm	54.6 mm	36.3 mm	37.3 mm
Percent of Nipher		52%	35%	36%
1995-1996 (3 Oct. 1995-June 3, 1996)	84.1 mm	49.3 mm	28.7 mm	23.9 mm
Percent of Nipher		58%	34%	28%
1996-1997 (3 Oct. 1996-5 June 1997)	80.8 mm	30.0 mm	10.4 mm	7.9 mm
Percent of Nipher		37%	13%	10%
1997-1998 (1 Oct. 1997-2 June 1998)	89.4 mm	45.5 mm	18.3 mm	29.5 mm
Percent of Nipher		51%	20%	33%
1998-1999 (1 Oct. 1998-2 June 1998)	113.8 mm	59.9 mm	36.6 mm	38.9 mm
Percent of Nipher		53%	32%	34%
1999-2000 (1 Oct. 1999-31 May 2000)	92.2 mm	62.2 mm	28.7 mm	21.1 mm
Percent of Nipher		68%	31%	23%
2000-2001 (1 Oct. 2000-31 May 2001)	75.2 mm	40.1 mm	22.6 mm	25.9 mm
Percent of Nipher		53%	30%	34%
2001-2002 (1 Oct. 2001-1 May 2002)	57.2 mm	–	16.5 mm	11.9 mm
Percent of Nipher		–	29%	21%
2002-2003 (1 Oct. 2002-31 May 2003)	73.4 mm	41.2 mm	29.5	27.4 mm
		56%	40%	37%

Acknowledgment. Appreciation is expressed to D. Endres, Station Chief at Barrow, Alaska, for servicing the precipitation gauges and collecting the snow samples.

REFERENCES

Alter, S.C. (1937), Shield storage precipitation gauges, *Mon. Weather Rev.*, *65*, 262-265.

Goodison, B.E., W.R. Turner, and J.E. Metcalfe (1983), A Nipher-type shield for recording precipitation gauges, *Procceedings of the 5th Symposium on Meteorological Observations and Instrumentation*, pp. 2-126, Toronto, Ontario, Canada, Am. Meteorol. Soc., Boston, MA.

Hanson, C.L. (1988), Precipitation measured by gauges protected by the Wyoming shield and dual-gauge system, *Procceedings of the 56th Western Snow Conference*, pp. 174-177, Kalispell, Montana, Colo. State Univ., Fort Collins.

Investigation of Chemical Transfer Processes between Atmosphere and Snow at South Pole

JOSEPH R. MCCONNELL
Division of Hydrologic Sciences, Desert Research Institute, Reno NV 89512

ROGER C. BALES
University of California, Merced 95344

Through a cooperative agreement with CMDL, we have been making year-round measurements of the hydrogen peroxide (H_2O_2) concentration in the surface and near-surface snow at the South Pole since November 1994 and measurements of the nitrate (NO_3^-) concentration since January 2000. Similar measurements for the HFC degradation product trifluoroacetate (TFA) were added recently. These year-round measurements in the surface snow complement the more intensive, summertime measurements in the atmosphere and in the snow pits and shallow cores. The summer sampling at the South Pole and all sample analyses are conducted under National Science Foundation (NSF) grants.

Oxidation by OH is the primary atmospheric sink for many environmentally important gases including methane (CH_4), carbon monoxide (CO), and halogenated hydrocarbons. Because of its very short lifetime, OH is not preserved in the snow and ice. Hydrogen peroxide (H_2O_2) is a sink for OH because it is preserved in the snow and ice. Changes in the concentrations of H_2O_2 archived in ice sheets offer the potential to reconstruct past atmospheric concentrations of H_2O_2 and, hence, OH. Nitrate and trifluoroacetate concentrations are also related to OH. Recent studies at South Pole suggest that the NO_x chemistry in the boundary layer is closely linked to the photochemistry in the near surface snow [*Chen et al*., 2001]. However, use of the glaciochemical archive requires a quantitative understanding of the processes that control atmosphere to snow transfer and the preservation of these chemical species in polar environments.

Results of the nearly continuous, year-round surface-snow sampling H_2O_2: November 1994 through January 2003, and NO_3^-: January 2000 through January 2003 are shown in Figure 1. Replicate samples are collected at each sampling period and error bars show the variability (1 σ) of the concentration between replicates. There are distinct annual cycles in both the H_2O_2 and the NO_3^- concentrations in the surface snow.

The annual cycle in H_2O_2 results from a combination of very strong changes in atmospheric concentration of H_2O_2 throughout the year [*Stewart and McConnell*, 1999], a strong annual temperature cycle at South Pole, and a highly nonlinear partitioning of the H_2O_2 between air and snow as a function of temperature [*Conklin et al*., 1993; *McConnell et al.*, 1997]. Because deposition of H_2O_2 is reversible (a fraction of the deposited H_2O_2 cycles between the snow and the air until the snow is cut off from the atmosphere by burial), preservation is strongly dependent on depositional parameters such as temperature, snow accumulation rate, and timing [*McConnell*, 1997; *McConnell et al*., 1998; *Hutterli et al.,* 2001, 2003a, 2003b]. The net result is that while we have measured a strong decrease in H_2O_2 concentration in firn cores from the South Pole

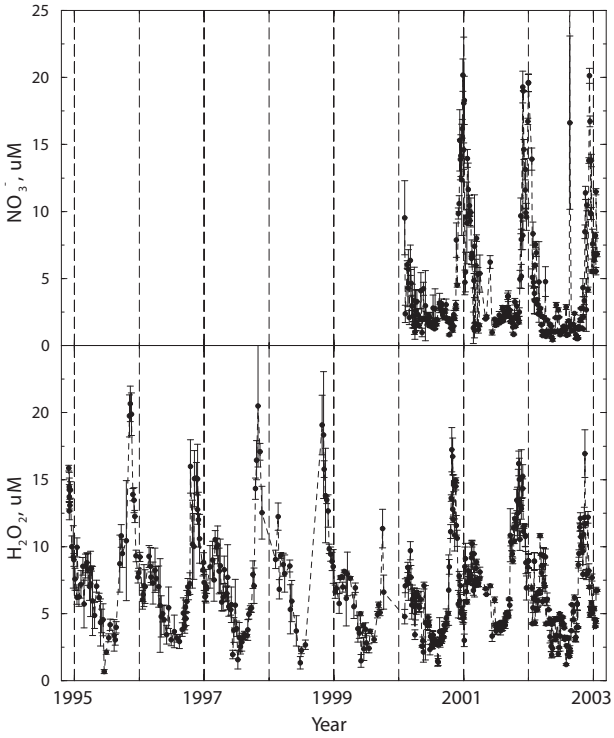

Figure 1. Hydrogen peroxide (H_2O_2) and nitrate (NO_3^-) in surface snow at South Pole. Error bars show one standard deviation in replicate measurements.

representing snow deposited over the past ~30 years, much of the observed decrease is likely to be the result of a slow release of H_2O_2 from supersaturated layers near the surface. The decrease with depth is pronounced at South Pole due to the relatively cold temperatures slow diffusion-controlled release of H_2O_2 from the snow pack, and because the low snow accumulation rates allow exchange with the atmosphere for many years after the snow is deposited.

Interpretation of the annual cycle in surface snow nitrate concentration is ongoing, and it is as yet unclear what roles temperature-driven partitioning, snow pack photochemistry, and seasonality in atmospheric concentration play in determining the surface snow concentration. However, concentrations in ice cores from South Pole are lower than many other polar locations with average concentrations of approximately 1.6 μmol and peak concentrations generally less than ~2.5 μmol over recent decades. Surface snow concentrations (Figure 1) averaged ~5 μmol over

the past 3 years with summer peak concentrations greater than 20 μmol, so only ~30% and ~13% of the NO_3^- found in the surface snow throughout the year and during the summer is preserved in the deeper snow pack, respectively.

Formaldehyde (HCHO) concentrations also provide information on the atmospheric oxidation capacity, and HCHO studies in the air and snow at the South Pole are integral to our overall research effort. Results of recent snow pit and shallow core studies at the South Pole are in agreement with similar studies in Greenland and other Antarctic locations and show HCHO deposition is reversible and the exchange with the atmosphere is much greater than for H_2O_2 [*Hutterli et al*., 2003a, 2003b]. HCHO concentrations in snow samples are time sensitive, thereby precluding year-round surface snow sampling by onsite CMDL personnel.

Year-round surface snow studies at the South Pole have recently been expanded to include sampling for TFA. TFA is the primary atmospheric degradation product of the CFC replacement HFC-134A, and there is concern about the environmental consequences in a buildup of this strongly hydrophilic compound in natural waters. The South Pole is a particularly appropriate location to carry out such sampling since atmospheric measurements of the primary precursor, HFC-134A, and other related compounds have been made by CMDL since ~1994 [*Montzka et al*., 1996]. Moreover, measurements of HFC-134a in the firn air at the South Pole have recently been reported [*Butler et al*., 1999]. As with the H_2O_2 and NO_3^- studies, year-round sampling by onsite CMDL personnel complements the more intensive summer snow pit sampling conducted under NSF funding.

The year-round South Pole data made possible through the cooperative agreement with CMDL are also important for interpreting similar H_2O_2, HCHO, NO_3^-, and TFA data from the snow pits and shallow cores collected at other polar locations such as the summertime sampling in West Antarctica as part of the International Trans-Antarctic Scientific Expedition (ITASE - http://www.secretsoftheice.org/) [*Frey et al.*, 2001, 2003]. Similar year-round surface snow and boundary layer sampling at Summit, Greenland (www.geosummit.org) provides a Northern Hemisphere analog for the South Pole studies.

REFERENCES

Butler, J.A., M. Battle, M.L. Bender, S.A. Montzka, A.D. Clarke, E.S. Saltzman, C.M. Sucher, J.P. Severinghaus, and J.W. Elkins (1999), A record of atmospheric halocarbons during the twentieth century from polar firn air, *Nature*, *399*, 749-755.

Chen, G., D. Davis, J. Crawford, J.B. Nowak, F. Eisele, R.L. Mauldin III, D. Tanner, M. Buhr, R. Shetter, B. Lefer, R. Arimoto, A. Hogan, and D. Blake (2001), An investigation of South Pole HOx chemistry: Comparison of model results with ISCAT observations, *Geophys. Res. Lett.*, *28*, 3633-3636.

Conklin, M.H., A. Sigg, A. Neftel, and R.C. Bales (1993), Atmosphere-snow transfer function for H_2O_2: Microphysical considerations, *J. Geophys. Res.*, *98*(D10), 18,367-18,376.

Frey, M., J. McConnell, R. Bales, and M. Hutterli (2001), Peroxides and formaldehyde in West Antarctica: Atmospheric and snow chemistry measurements along the ITASE traverse, *Eos Trans. AGU,* OS51B-12.

Frey, M.M., J.R. McConnell, M.A. Hutterli, D. Belle-Oudry, and R.C. Bales (2003), Hydrogen peroxide and formaldehyde in snow and the atmosphere in West Antarctica: Implications for atmospheric boundary layer chemistry and interpretation of ice core records, European Geophysical Society XXVIII General Assembly, EAE03-A-03165.

Hutterli, M.A., McConnell, J.R., R.W. Stewart, H.–W. Jacobi, and R.C. Bales (2001), Impact of temperature-driven cycling of hydrogen peroxide (H2O2) between air and snow on the planetary boundary layer, *J. Geophys. Res.*, *106*(D14), 15395-15404.

Hutterli, M.A., J.R. McConnell, R.C. Bales, and R.W. Stewart (2003a), Sensitivity of hydrogen peroxide (H_2O_2) and formaldehyde (HCHO) in snow to changing environmental conditions: Implications for ice-core records, *J. Geophys. Res., 108*(D1), 4023.

Hutterli, M.A., J.R. McConnell, G. Chen, R.C. Bales, D. Davis, and D.H. Lenschow (2003b), Formaldehyde and Hydrogen Peroxide in Air, Snow and Interstitial Air at South Pole, *Atmos. Environ.,* in press.

McConnell, J.R. (1997), Investigation of the atmosphere-snow transfer process for hydrogen peroxide, Ph.D. Dissertation, Dept. Hydrol. and Water Res., Univ. of Arizona.

McConnell, J.R., J.R. Winterle, R.C. Bales, A.M. Thompson and R.W. Stewart (1997), Physically based inversion of surface snow concentrations of hydrogen peroxide to atmospheric concentrations at South Pole, *Geophys. Res. Lett.*, *24*(4), 441-444.

McConnell, J.R., R.C. Bales, R.W. Stewart, A.M. Thompson, M.R. Albert, and R. Ramos (1998), Physically Based Modeling of Atmosphere-to-Snow-to-Firn Transfer of Hydrogen Peroxide at South Pole, *J. Geophys. Res.*, *103*(D9), 10,561-10,570.

Montzka, S.A., J.H. Butler, R.C. Myers, T.M. Thompson, T.H. Swanson, A.D. Clarke, L.T. Lock, and J.W. Elkins (1996), Decline in the tropospheric abundance of halogen from halocarbons: Implications for stratospheric ozone depletion, *Science*, *272*, 1318-1322.

Stewart, R. and J. McConnell (1999), Antarctic photochemistry: Uncertainty analysis, *Eos Trans. AGU*, A41A-12.

Measurement of Net Ecosystem CO_2 Exchange Using Eddy Covariance Technique in Arctic Wet Coastal Sedge Tundra

WALTER C. OECHEL AND HYOJUNG KWON
Global Change Research Group, San Diego State University, California 92182

STEVE RUNNING AND FAITH-ANN HEINSCH
Numerical Terradynamic Simulation Group, University of Montana, Missoula, 59812

INTRODUCTION

The Arctic represents a model biome in which to study the effects of climate variability and change on ecosystem function because of the sensitivity of Arctic ecosystems to global warming and climate change. The demonstrated importance of variance in high-latitude temperature and hydrology on the magnitude and direction of the net ecosystem CO_2 exchange (NEE) and the high heterogeneity of spatial and temporal variances over the Arctic make this an important and tractable ecosystem for study.

The Barrow region has been a focal point of ecosystem research such as the International Biological Programme (IBP) and Research on Arctic Tundra Environment, funded by the National Science Foundation (NSF), as well as atmospheric research (NOAA) for more than 35 years [*Batzli*, 1980; *Brown et al*., 1980; *Chapin et al*., 1980; *Miller et al*., 1983; *Oechel et al*., 1993]. The Global Change Research Group (GCRG) at San Diego State University has conducted measurements of mass and energy fluxes in the Barrow region since 1998. The GCRG's current Study of Environmental Arctic Change (SEARCH) project, funded by NSF, includes three flux measurement sites in the Arctic region; Barrow is one of these sites.

One of the primary objectives of the SEARCH project is to determine the patterns and controls on interannual variability in NEE at different Arctic ecosystem types and to determine the scaled, temporal, and spatial patterns of regional flux values from eddy covariance towers using remotely sensed, Moderate-Resolution Imaging Spectroradiometer (MODIS) compatible data sets. As a preliminary step toward accomplishing these objectives, it is important to quantify NEE and to assess the controlling factors on NEE. The data presented here provide a baseline for quantification of seasonal NEE and for comparison of NEE measured with an eddy covariance tower against NEE predicted by MODIS models.

METHOD

Eddy Covariance Measurements

Measurement of net NEE was made using eddy covariance techniques [*Baldocchi et al*., 1988] from a tower at a height of 5 m for the wet coastal sedge tundra site. Fluctuations in vertical, streamwise, and lateral wind speed along with fluctuations in temperature were measured at 10 Hz using a three-dimensional sonic anemometer (Model R3, Gill Instruments, Lymington, England) for the three sites. An open-path infrared gas analyzer (IRGA; Model LI-7500, LI-COR, Inc., Lincoln, Nebraska) was used to measure CO_2 and water vapor fluctuations at the sites. Half-hour eddy covariances and statistics were calculated online from 10-Hz raw data, and these data were stored on a laptop computer. CO_2 and water vapor fluxes were corrected for the variation in air density due to simultaneous transfers of water vapor and sensible heat according to the work of *Webb et al*. [1980]. Environmental measurements such as net radiation, photosynthetically active radiation, and air temperature were conducted along with the NEE measurements. The environmental data are averaged at every half-hour and stored in a data logger (Model 23X, Campbell Scientific Inc., Logan, Utah). The measurements of surface soil moisture and active layer depth were conducted once every week throughout the growing season (June through August).

Integration of the MODIS Modeling with the Tower Flux Measurements

The measurements of NEE collected at Barrow for 2001 and 2002 were compared to the results from the MODIS products such as gross primary productivity (GPP), NEE, and ecosystem respiration (ER). After the MODIS model was tuned to the environmental conditions and the amplitude of carbon balance at the Barrow site, it was used to estimate the seasonal and annual carbon balance for the Barrow site. This MODIS model, which has a fundamental link with the Biome-BGC model, was able to predict long-term (30 year: 1970 to 2000) carbon balance for the Barrow site [*Heinsch et al*., 2003].

RESULTS

The seasonal trends of the daily NEE at the Barrow site for 2002 and 2003 are illustrated in Figure 1. The daily NEE in the 2002 growing season ranged from -2.9 g C m^{-2} d^{-1} (carbon sink) to +0.87 g C m^{-2} d^{-1} (carbon source), while the daily NEE in the 2003 growing season ranged from -4.3 g C m^{-2} d^{-1} to 2.3 g C m^{-2} d^{-1}. Because of the early snowmelt (Day of Year 144; Robert Stone, personal communication, 2003) and high Normalized Difference Vegetation Index (NDVI) in the early growing season in 2002, considerable carbon uptake took place in the early growing season with a maximum carbon uptake of -2.9 g C m^{-2} d^{-1}. Cumulative seasonal carbon at the Barrow site was 60.8 g C m^{-2} $season^{-1}$ and 58.5 g C m^{-2} $season^{-1}$ during 2002 and 2003, respectively.

Figure 2 shows a 30-year model run of the GPP, NEE, and ER generated using the ecosystem process model Biome-BGC (version 4.1.1) for Barrow. Long-term estimates of air

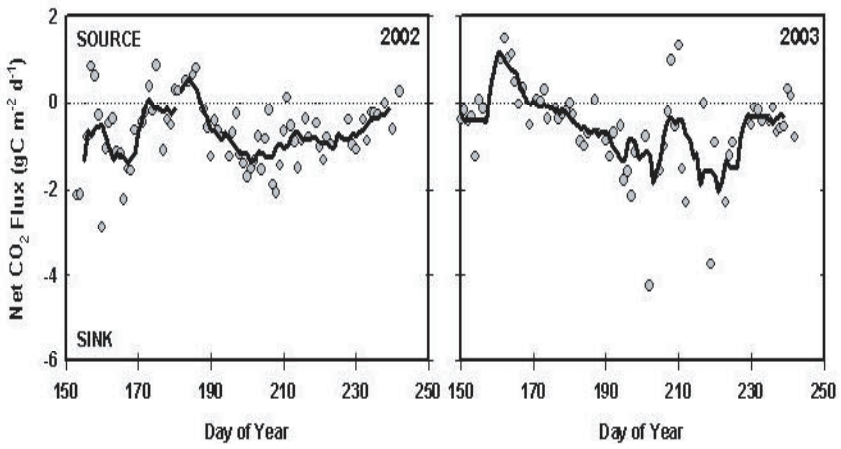

Figure 1. The seasonal cumulative NEE at the Barrow site during the 2002 and 2003 growing seasons. Open circles indicate the daily NEE, while the solid line indicates a 7 day-running mean.

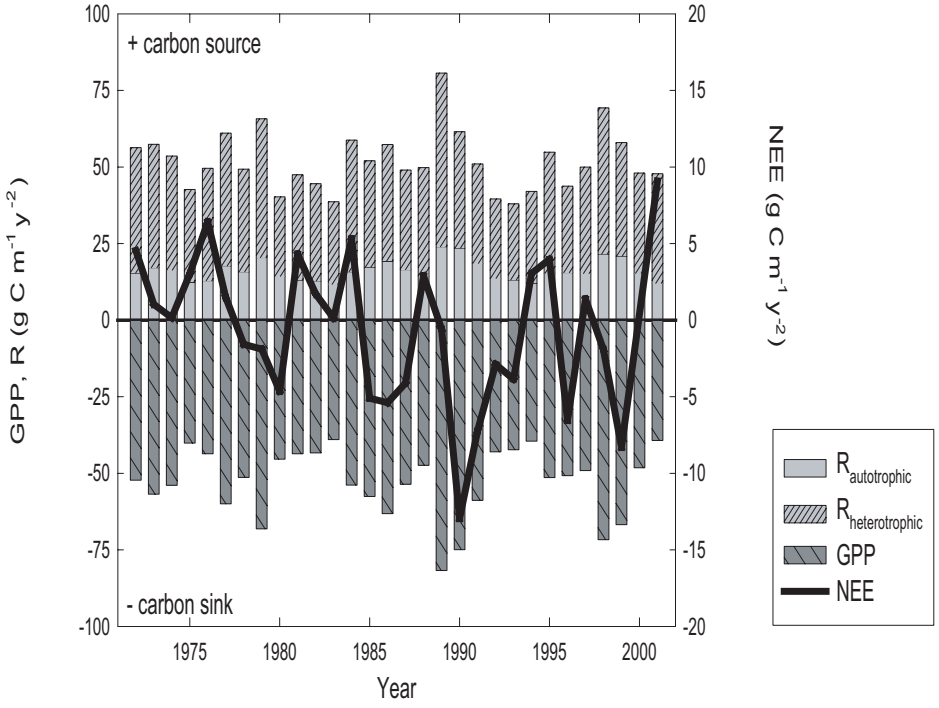

Figure 2. Thirty-year model runs of gross primary production (GPP), net ecosystem CO_2 exchange (NEE), and respiration ($R_{autotrophic}$ and $R_{heterotrophic}$) generated by BIOME-BGC for Barrow, Alaska.

temperature and precipitation, based on records obtained from the W. Rogers Airport, Barrow, Alaska, were obtained by linear regression of air temperature data against tower measurements and the use of the Daymet model for estimates of precipitation [www.daymet.org; *Thornton et al*., 2000]. The results indicate that (1) the Barrow site was a slight carbon sink over the last 30 years and (2) the Barrow site could become a carbon source if warming and drying conditions continue.

Acknowledgment. The authors thank the CMDL BRW staff (Dan Endres and Don Neff) for providing facilities, helping with tower maintenance, and assisting periodically with the instrumentation and data acquisition computers.

References

Baldocchi, D.D., B.B. Hicks, and T.P. Meyers (1988), Measuring biosphere-atmosphere exchanges of biologically related gases with micrometeorological methods, *Ecology*, *69*, 1331-1340.

Batzli, G.O. (1980), Patterns of vegetation and herbivory in Arctic tundra: Results from the Research on Arctic Tundra Environment (RATE) program, *Arc. Alp. Res., 12*, 401-578.

Brown, J, P.C. Miller, L.L. Tieszen, and F.L. Bunnell (Eds.) (1980), *An Arctic Ecosystem: The Coastal Tundra at Barrow, Alaska*, 571 pp., Dowden, Hutchinson, and Ross, Stroudsburg, PA.

Chapin, F.S. III, P.C. Miller, W.D. Billings, and P.I. Coyne (1980), Carbon and nutrient budgets and their control in coastal tundra, in *An Arctic Ecosystem: The Coastal Tundra at Barrow, Alaska,* edited by J. Brown, P.C. Miller, L.L. Tieszen, and F.L. Bunnell, pp. 458-482, Dowden, Hutchinson and Ross, Stroudsberg, PA.

Heinsch, F.A., M. Reeves, C.F. Bowker, P. Votava, S. Kang, C. Milesi, M. Zhao, J. Glassy, J.S. Kimball, R.R. Nemani, and S.W. Running (2003), *User's Guide: GPP and NPP (MOD17A2/A3) Products, NASA MODIS Land Algorithm*, NTSG, Missoula, MT.

Miller, P.C., R. Kendall, and W.C. Oechel (1983), Simulating carbon accumulation in northern ecosystems, *Simuao.*, *40*, 119-131

Oechel, W.C., S.J. Hastings, G.L. Vourlitis, M. Jenkins, G. Riechers, and N. Grulke (1993), Recent change of Arctic tundra ecosystems from a net carbon dioxide sink to a source, *Nature*, *361*, 520-523.

Thornton, P.E., H. Hasenauer, and M.A. White (2000), Simultaneous estimation of daily solar radiation and humidity from observed temperature and precipitation: An application over complex terrain in Austria, *Agri. For. Meteorol. 104*, 255-271.

Webb, E.K., G.I. Pearman, and R. Leuning (1980), Corrections of flux measurements for density effects due to heat and water vapor transfer, *Q. J. R. Meteorol. Soc., 106*, 85-100.

Advanced Global Atmospheric Gases Experiment (AGAGE)

R. G. PRINN
Massachusetts Institute of Technology, Cambridge, 02139

R. F. WEISS
Scripps Institution of Oceanography, University of California, La Jolla, 92093

D. M. CUNNOLD
Georgia Institute of Technology, Atlanta, 30332

P. J. FRASER
CSIRO, Division of Atmospheric Research, Victoria, Australia 3195

P. G. SIMMONDS
University of Bristol, School of Chemistry, United Kingdom BS8 1TS

INTRODUCTION

The Advanced Global Atmospheric Gases Experiment (AGAGE) and its predecessors provide continuous high-frequency gas chromatographic measurements of biogenic and anthropogenic gases that are carried out at globally distributed sites to quantitatively determine the source and sink strengths and propagation of a large number of chemically and radiatively important long-lived gases. The program started in 1978 and is divided into three parts associated with changes in instrumentation: the Atmospheric Lifetime Experiment (ALE), the Global Atmospheric Gases Experiment (GAGE), and AGAGE. These three successive automated high-frequency in situ experiments have documented the long-term behavior of measured concentrations of these important gases over the past 25 years and show both the evolution of latitudinal gradients and the high-frequency variability of sources and circulation.

AGAGE began during the 1993–1996 time period and continues to the present. It has different instrumental components. First, a highly improved gas chromatographic system measures five biogenic/anthropogenic gases (CH_4, N_2O, $CHCl_3$, CO, and H_2) and five anthropogenic gases (CCl_3F, CCl_2F_2, CH_3CCl_3, CCl_2FCClF_2, and CCl_4). Each species is measured 36 times per day using electron capture detectors (ECDs), flame ionization detectors (FIDs), and mercuric oxide reduction detectors (MRDs); the last detector is for CO and H_2 and is currently present only at two of the stations, Mace Head, Ireland, and Cape Grim, Tasmania. Second, AGAGE is deploying new gas chromatographic-mass spectrometric (GC-MS) instrumentation throughout its network in order to measure a wide range of hydrochlorofluorocarbons and hydrofluorocarbons such as CH_2FCF_3 (HFC-134a), CH_3CCl_2F (HCFC-141b), CH_3CClF_2 (HCFC-142b), etc., methyl halides (CH_3Cl, CH_3Br, CH_3I), halons ($CBrF_3$, $CBrClF_2$), and perfluorinated compounds including CF_4, C_2F_6 (PFC-116) and SF_6 that are either serving as interim or permanent alternatives to the chlorofluorocarbons and other long-lived halocarbons regulated by the Montreal Protocol [*UNEP*, 2003] or are important because of their radiative properties [*IPCC*, 2001]. At present, GC-MS instruments using Peltier-cooled trapping systems are measuring all but the most volatile of these compounds at the Mace Head and Cape Grim stations, and the new Medusa GC-MS systems that use cryogenic refrigeration trapping and refocusing injection systems are now being deployed, beginning with these same stations. AGAGE also encompasses the development and use of new, more accurate, absolute calibrations for measuring many of the gases.

The ALE, GAGE, and AGAGE stations have been located in five globally distributed localities: (1) Ireland: first at Adrigole, 52°N, 10°W (1978–1983), then at Mace Head, 53°N, 10°W (1987–present); (2) U.S. West Coast: first at Cape Meares, Oregon, 45°N, 124°W (1979–1989), then at Trinidad Head, California, 41°N, 124°W (1995–present); (3) Ragged Point, Barbados, 13°N, 59°W (1978–present); (4) Cape Matatula, American Samoa, 14°S, 171°W (1978–present); and (5) Cape Grim, Tasmania, 41°S, 145°E (1978–present).

Of special significance is the AGAGE operation at Samoa that enables a direct intercomparison with the similar real-time measurements (and also with flask measurements) by the CMDL group. This intercomparison has been extremely valuable in helping us to quantify the net effects of calibration and instrument differences in the measurements by each program; therefore, the data from both the AGAGE and CMDL networks can be utilized in combination by theoreticians and modelers to investigate chemical and meteorological phenomena.

RECENT PROGRESS

The continuous measurement of methane since 1986 at GAGE/AGAGE stations was described in the work of *Cunnold et al.* [2002]. The measurements, combined with a 12-box atmospheric model and an assumed atmospheric lifetime of 9.1 years, indicate net annual emissions (emissions minus soil sinks) of 545 Tg CH_4, with a variability of only ±20 Tg from 1985 to 1997, but with an increase in the emissions in 1998 of 37 ± 10 Tg. The effect of OH changes inferred in the work of *Prinn et al.* [2001] is to increase the estimated methane emissions by approximately 20 Tg in the mid-1980s and to reduce them by 20 Tg in 1997, and by more thereafter. Using the 12-box model with transport constrained by the GAGE/AGAGE chlorofluorocarbon measurements, we calculate that the proportion of CH_4 emissions coming from the Northern Hemisphere is between 73% and 81%, depending on the OH distribution used. The 2-D model, combined with the annual

cycle in OH from the work of *Spivakovsky et al.* [2000], provides an acceptable fit to the observed 12-month cycles in methane. The trend in the amplitude of the annual cycle of methane at Cape Grim infers a trend in OH from 30°S to 90°S of 0 ± 5% per decade from 1985 to 2000, in qualitative agreement with the work of *Prinn et al.* [2001] for the Southern Hemisphere.

We carried out a critical evaluation of emissions of potential new gases for OH estimation [*Huang and Prinn*, 2002]. Accurate determination of global and regional tropospheric OH concentrations is very important and can be achieved by measuring the gases that react with OH and whose emissions are well known. CH_3CCl_3 was used for this purpose. Prior studies show that three of the new chlorofluorocarbon (CFC) substitutes, HFC-134a (CH_2FCF_3), HCFC-141b (CH_3CCl_2F), and HCFC-142b (CH_3CClF_2), could potentially be used to derive accurate global averages of OH concentrations in the future, provided the industrial emissions of these gases can be reliably estimated. As a test of available emission estimates, we optimally determined the monthly emissions for these three gases using global measurements from the CMDL and AGAGE networks. We conclude that the current emission estimates by the Alternative Fluorocarbon Environmental Assessment Study (AFEAS) for HCFC-142b and HCFC-141b need to be increased by 18% over the 1992-2000 period and by 10% over the 1993-2000 period, respectively, while the emissions of HFC-134a (from 1993 to 2000) are only 4% more than those yielding the best agreement with atmospheric observations. Estimates of global-average OH concentrations using measurements and AFEAS emissions differ statistically from the average OH derived from CH_3CCl_3 for HCFC-141b and HCFC-142b but not for HFC-134a. On the other hand, OH trends deduced from all three HCFC/HFC gases are implausibly large, implying problems with the AFEAS estimates of the temporal variations in their emissions. As the viability of CH_3CCl_3 for estimating OH declines in the future, additional evaluations of the emissions and OH kinetics of HCFC-141b, HCFC-142b, and HFC-134a have a high priority.

AGAGE observations of methyl bromide and methyl chloride at Mace Head, Ireland, and Cape Grim, Tasmania, in 1998-2001 were reported in the work of *Simmonds et al.* [2004]. At Mace Head, both gases have well-defined seasonal cycles with similar average annual decreases of 3.0% yr^{-1} (CH_3Br) and 2.6% yr^{-1} (CH_3Cl), and mean Northern Hemisphere baseline mole fractions of 10.4 ppt and 535.7 ppt, respectively. We used a Lagrangian dispersion model and local meteorological data to segregate the Mace Head observations into different source regions and to interpret the results in terms of the known sources and sinks of these two key halocarbons. At Cape Grim, CH_3Br and CH_3Cl also show annual decreases in their baseline mixing ratios of 2.5% yr^{-1} and 1.4% yr^{-1}, respectively. Mean baseline mole fractions were 8.0 ppt (CH_3Br) and 541.1 ppt (CH_3Cl). Although CH_3Cl has a strong seasonal cycle, there is no well-defined seasonal cycle in the Cape Grim CH_3Br record. The fact that both gases are steadily decreasing in the atmosphere at both locations implies that a global-scale change occurred that is affecting a common, major source of both gases (possibly biomass burning) and/or their major sink process (destruction by hydroxyl radical).

Oxidation processes have played a major role in the evolution of the atmosphere, and the oxidizing capacity of the atmosphere has been critically evaluated [*Prinn*, 2003a, 2003b]. Observations of trace gases in AGAGE and elsewhere from 1978-2003 provide important constraints on the atmosphere's major oxidizing free radical OH. Annually, OH removes about 3.7 Pg of trace gases from the atmosphere. Chemicals in ice cores have recorded some information about the oxidizing capacity of past atmospheres. Models have been developed for fast photochemistry and for coupled chemical and transport processes that explain some of the observations, but there are important discrepancies between models and observations for OH and O_3 that still need to be resolved.

The role of non-CO_2 trace gases in climate change was reviewed and critically discussed [*Prinn*, 2004c, 2004d]. Current global emissions of these trace gases, expressed as equivalent amounts of carbon in CO_2 using global warming potentials (GWPs) with a 100-year lifetime, are 3.8, 2.1, and 1.5 PgC equivalent for CH_4, N_2O, and CO respectively. This accentuates the importance of measuring these gases and understanding their global budgets. Estimation of the emissions of these and other gases using AGAGE and other data has been critically reviewed [*Prinn*, 2002]. Estimations of CO_2, CH_4, N_2O, and $CHCl_3$ emissions from Europe using the AGAGE Mace Head data were reported in the work of *Biraud et al.* [2002]. European emissions of halogenated greenhouse gases were also determined from the AGAGE Mace Head data [*Greally et al.*, 2002; *O'Doherty et al.*, 2003]. Back-attribution techniques for inverting the AGAGE Ireland measurements to deduce European emissions were reported in the work of *Manning et al.* [2003]. Also, *Cox et al.* [2003] and *Cohan et al.* [2003] have identified regional sources of CH_3Cl, $CHCl_3$, CH_2Cl_2 and CH_3I using the AGAGE Tasmania observations.

The ALE/GAGE/AGAGE data are available through the DOE-CDIAC World Data Center (http://cdiac.esd.ornl.gov/, Dataset DB-1001).

Acknowledgments. In its initial years, the global network (ALE) was supported first by grants from the Chemical Manufacturers Association and later also by the Upper Atmospheric Research Program of the National Aeronautics and Space Administration (NASA). GAGE was subsequently supported by multiple grants from NASA. In its latest phase (AGAGE) support came (and comes) primarily from NASA (grants NAF5-12669 to MIT; and NAG5-12807 and NAG5-12806 to SIO) with important contributions also from the United Kingdom Department of the Environment, Food and the Rural Affairs (contracts PECD 1/1/130 and 7/10/154 and EPG 1/1/130 and 1/1/82 to Inscon), Commonwealth Scientific and Industrial Research Organisation (Australia), Bureau of Meteorology (Australia), and the Alternative Fluorocarbons Environmental Acceptability Study (AFEAS). Support for the Barbados station during GAGE/AGAGE has been shared approximately equally between NASA and NOAA. We also thank NOAA for their infrastructure support at the Samoa station by Cooperative Agreement.

REFERENCES

Biraud, S., P. Ciais, M. Ramonet, P. Simmonds, V. Kazan, P. Monfray, S. O'Doherty, G. Spain, and S.G. Jennings (2002), Quantification of carbon dioxide, methane, nitrous oxide and chloroform emissions over Ireland from atmospheric observations at Mace Head, *Tellus*, *Ser. B, 54,* 41-60.

Cohan, D.S., G.A. Sturrock, A.P. Biazar and P.J. Fraser (2003), Atmospheric methyl iodide at Cape Grim, Tasmania, from AGAGE observations, *J. Atmos. Chem.*, *44*, 131-150.

Cox, M.L., G.A. Sturrock, P.J. Fraser, S. Siems, P. Krummel, and S. O'Doherty (2003), Regional sources of methyl chloride, chloroform, and dichloromethane identified from AGAGE observations at Cape Grim, Tasmania, 1998-2000. *J. Atmos. Chem.*, *45*, 79-99.

Cunnold, D.M., L.P. Steele, P.J. Fraser, P.G. Simmonds, R.G. Prinn, R.F Weiss, L.W. Porter, R.L. Langenfelds, P.B. Krummel, H.J. Wang, L. Emmons, X.X. Tie, and E.J. Dlugokencky (2002), In situ measurements of atmospheric methane at GAGE/AGAGE sites during 1985-1999 and resulting source inferences, *J. Geophys. Res., 107*(D14), 10.1029/2001JD001226-4225.

Greally, B.R., P.G. Simmonds, S.J. O'Doherty, G. Nickless, A. McCulloch, S. Reimann, N. Schmidbauer, M. Maione, D.B. Ryall, R.G. Derwent, and A.J. Manning (2002), Observations of halogenated greenhouse gases and estimation of European source strengths, in *Non-CO_2 Greenhouse Gases: Scientific Understanding, Control Options, and Policy Aspects*, edited by J. van Ham et al., pp. 553-557, Millpress, Rotterdam.

Huang, J., and R.G. Prinn (2002), Critical evaluation of emissions for potential new OH titrating gases, J. *Geophys. Res., 107*(D24), 10.1029/2002JD002394-4784.

IPCC (Intergovernmental Panel on Climate Change), The Scientific Basis, in *Climate Change 2001: The Scientific Basis-Contribution of Working Group I to the Third Assessment Report of the Intergovernmental Panel on Climate Change*, edited by J. T. Houghton et al., 881 pp., Cambridge Univ. Press, New York.

Manning, A.J., D.B. Ryall, R.G. Derwent, P.G. Simmonds, and S. O'Doherty (2003), Estimating European emissions of ozone-depleting and greenhouse gases using observations and a modelling back-attribution technique, *J. Geophys. Res*., *108*(D14), 4405, doi:10.1029/2002JD002312.

O'Doherty, S., A. McCulloch, E. O'Leary, J. Finn and D. Cunningham (2003), Climate Change: Emissions of industrial greenhouse gases (HFCs, PFCs and sulphur hexafluoride), *ERTDI Rep. Ser. No. 10*, 81 pp., Environ. Prot. Agency, Wexford, Ireland.

Prinn, R.G. (2002), Verification of emissions by inverse modelling, in *Non-CO_2 Greenhouse Gases: Scientific Understanding, Control Options, and Policy Aspects*, edited by J. van Ham et al., pp. 511-515, Millpress, Rotterdam.

Prinn, R.G. (2003a), The cleansing capacity of the atmosphere, *Ann. Rev., Environ. and Resources*, *28*, 7.1-7.29.

Prinn, R.G. (2003b), Ozone, hydroxyl radical and oxidative capacity, in *Treatise on Geochemistry*, edited by K. Turekian and H. Holland, Chap. 1, Vol. 4, pp. 1-19, Pergamon, New York.

Prinn, R.G. (2004a), Non-CO_2 greenhouse gases, in *The Global Carbon Cycle: Integrating Humans, Climate, and the Natural World*, edited by C. Field and M. Raupach, *62*, pp. 205-216, Island Press, New York.

Prinn, R.G. (2004b), Atmospheric chemical change, air pollution, and climate, in *State of the Planet,* edited by C. Hawksworth and S. Sparks, AGU Monograph, in press.

Prinn, R.G., J. Huang, R.F. Weiss, D.M. Cunnold, P.J. Fraser, P.G. Simmonds, A. McCulloch, C. Harth, P. Salameh, S. O'Doherty, R.H.J. Wang, L. Porter, and B.R. Miller (2001), Evidence for substantial variations in atmospheric hydroxyl radicals in the past two decades, *Science*, *292*, 1882-1888.

Simmonds, P.G., R.G. Derwent, A.J. Manning, P.J. Fraser. P.B. Krummel, S. O'Doherty, R.G. Prinn, D.M. Cunnold, B.R. Miller, and H.J. Wang (2004), AGAGE Observations of methyl bromide and methyl chloride at Mace Head, Ireland, and Cape Grim, Tasmania, 1998-2001, *J. Atmos. Chem*., *47*, 243-269.

Spivakovsky, C.M., J.A. Logan, S.A. Montzka, Y.J. Balkanski, M. Foreman-Fowler, D.B.A. Jones, L.W. Horowitz, A.C. Fusco, C.A.M. Brenninkmeijer, M.J. Prather, S.C. Wofsy, and M.B. McElroy (2000), Three-dimensional climatological distribution of tropospheric OH: Update and evaluation, *J. Geophys. Res*., *105*, 8931-8980.

UNEP (United Nations Environment Programme) (2003), *Handbook for the International Treaties for the Protection of the Ozone Layer*, 6th Edition, Nairobi, Kenya, 398 pp.

Results from Simultaneously Measured Aerosol Chemical and Optical Properties at Barrow, Alaska

P. K. QUINN
NOAA PMEL, Seattle, Washington 98115-0070

J. A. OGREN AND E. ANDREWS
NOAA CMDL, Boulder, Colorado 80305-3328

G. E. SHAW
Geophysical Institute, University of Alaska, Fairbanks, 99775-6160

INTRODUCTION

The Arctic late winter/early spring maximum in aerosol light scattering, absorption, and mass concentration is a well-documented phenomenon known as Arctic haze. Several seasonal variations contribute to the development of Arctic haze including stronger transport from the midlatitudes to the Arctic [e.g., *Barrie et al*., 1989; *Iverson and Joranger*, 1985] and weaker pollutant removal through wet deposition in the winter and spring [e.g., *Barrie et al*., 1981; *Heintzenberg and Larssen*, 1983]. Arctic haze has been the subject of much study because it may change the solar radiation balance of the Arctic, affect visibility, and provide a source of contaminants to Arctic ecosystems.

The research goals discussed here are twofold: (1) to assess long-term trends in Arctic haze and to ascertain the cause of the observed trends by continuous measurements of aerosol properties at Barrow, Alaska, and (2) to characterize means, variabilities, and trends of climate forcing properties of different aerosol types in order to assess the impact of Arctic haze on the region's radiation budget. To this end, measurements of aerosol chemical composition are made by the NOAA Pacific Marine Environment Laboratory (PMEL) in conjunction with the measurements of aerosol optical properties made by CMDL.

METHODS

Details about the measurement of aerosol chemical composition at Barrow can be found in the work of *Quinn et al.* [2002]. Briefly, particles with aerodynamic diameters between 1 and 10 μm are collected on a Tedlar film. Particles with diameters less than 1 μm pass through the impactor to a filter carousel housing eight Millipore Fluoropore filters (1.0 μm pore size). Computer-controlled solenoid valves downstream of the filters open and close sequentially so that one filter is sampled at a time. Submicron filter samples are collected over a period of 1 to 5 days depending on the time of year and the aerosol loading. One filter serves as a sampling blank and is exposed to sample air for 10 seconds. One super micron sample is collected with the impactor during the time it takes to sample all of the submicron filters in the carousel. After collection, samples are shipped to PMEL for ion chromatography and gravimetric analysis. Details of the measurement of aerosol optical properties can be found in the work of *Delene and Ogren* [2002].

RESULTS

Annual Cycle of Aerosol Chemical Composition

This work has resulted in the longest reported record of simultaneously measured aerosol chemical and optical properties at Barrow, Alaska. Measurements have been made from October of 1997 to present. Results to date include [*Quinn et al.*, 2002]: (1) Submicron non-sea-salt $SO_4^=$, K^+, Mg^{+2}, and Ca^{+2}, and NH_4^+ peak in winter and early spring corresponding to the arrival and persistence of Arctic haze. Non-sea salt $SO_4^=$ is a tracer of industrial pollution, nss K^+ of forest fires or biomass burning, and nss Mg^{+2} and Ca^{+2} of dust. Submicron sea salt displays a similar annual cycle presumably because of long range transport from the northern Pacific Ocean. Super micron sea salt peaks in the summer when there is a corresponding decrease in sea ice extent. Submicron and super micron MSA^- peak in the summer because of a seasonal increase in the flux of dimethylsulfide from the ocean to the atmosphere. (2) A correlation of MSA^- and particle number concentrations (r^2 = 0.8) suggests that summer time particle production is associated with biogenic sulfur. This result is confirmed by the relatively small size of the particles, as would be expected for newly formed particles. Size information was obtained from the multiwavelength light scattering measurements. (3) Continuous measurements of aerosol ionic chemical composition and light scattering indicate sea salt is dominant in controlling light scattering during the winter, non-sea salt $SO_4^=$ dominates in the spring, and both play a role in the summer.

Long Term Trends

With 5 years of chemical data from Barrow we are able to start comparing the trends in aerosol chemical composition and optical properties. Through this analysis we have determined the following: (1) Based on 5 years of chemical composition measurements at Barrow (1998–2002), there is a trend of increasing aerosol mass (Figure 1) over that period. The increase in aerosol mass appears to be because of the "residual" or chemically unanalyzed mass (most likely composed of organic species and/or dust) rather than nss sulfate. Within this trend of increasing mass, there are two peaks in mass concentration each year. The first occurs in January and the second in April. In order to explain the trend of increasing mass and its annual bimodal structure, it is essential that we determine the chemical composition of the residual mass. (2) The trend in increasing aerosol mass concentration corresponds

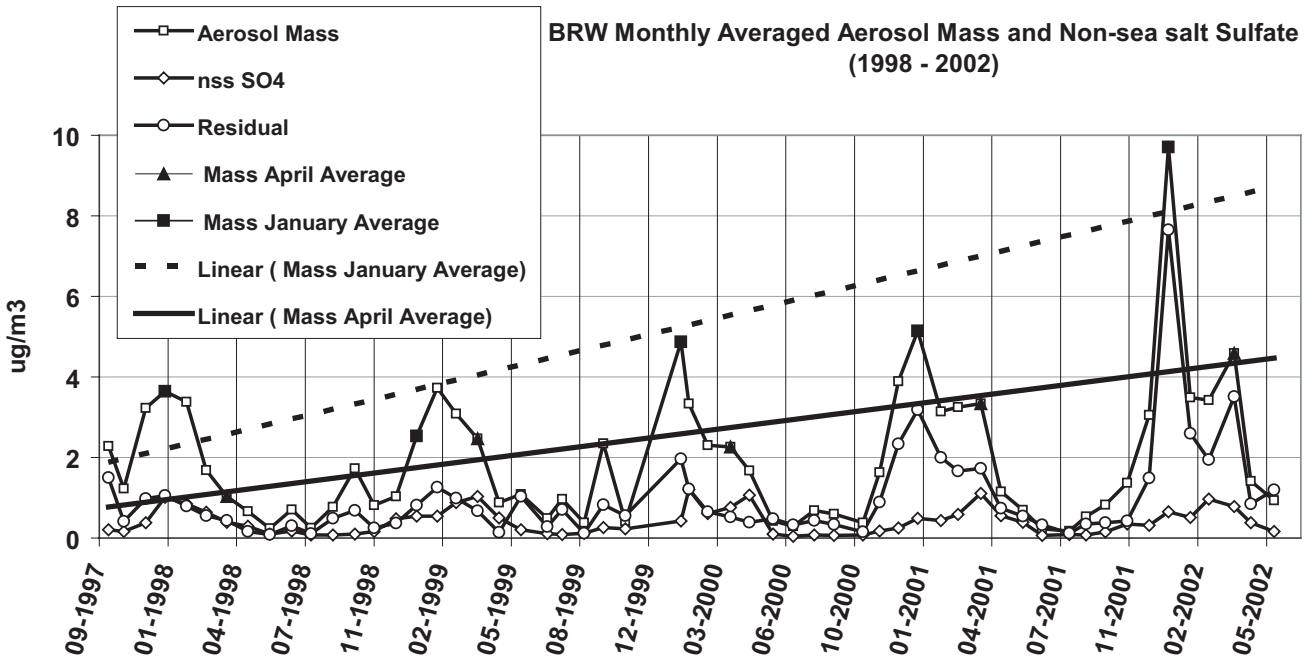

Figure 1. The trend of increasing submicron aerosol mass concentration from 1997 to 2002 measured at Barrow, Alaska. There is a corresponding trend of increasing concentration in the residual or chemically unanalyzed mass but not in nss sulfate. Also evident are two periods of peak concentrations (January and April) that occur each Arctic haze season.

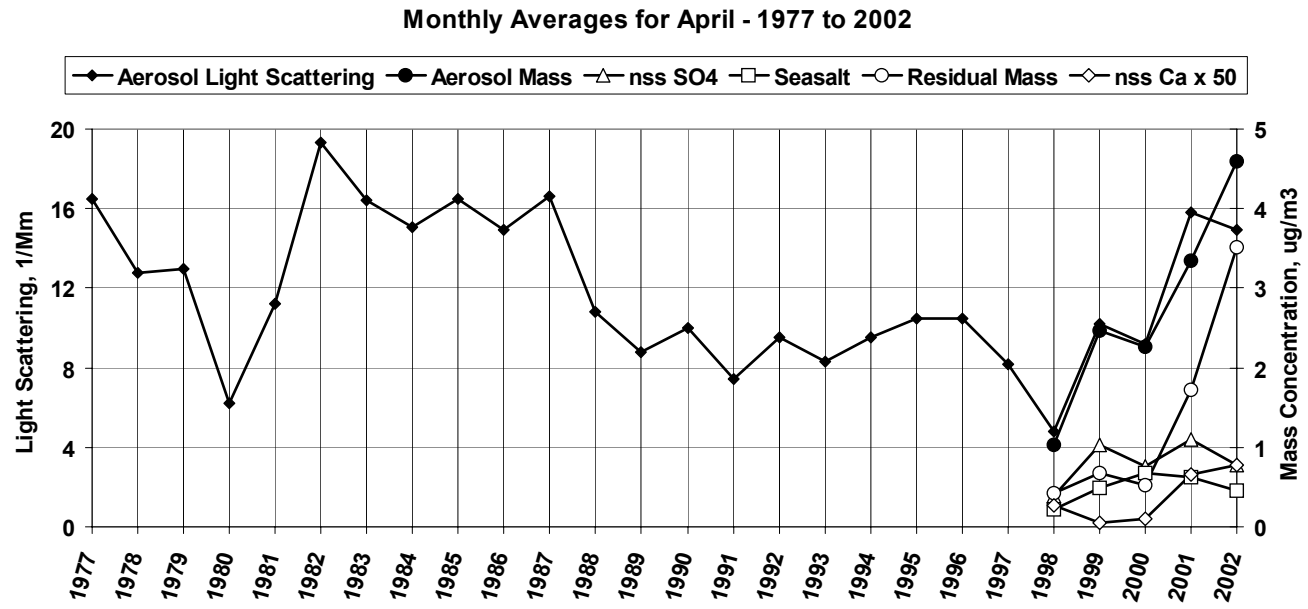

Figure 2. Monthly averages for April of aerosol light scattering (courtesy of CMDL), aerosol mass concentration, and the concentrations of nss $SO_4^=$, sea salt, residual mass, and nss Ca^{+2} (×50), which is a proxy for dust.

to the trend of increasing light scattering by aerosols over the past 5 years (Figure 2). Based on these data, it does not appear as if sea salt or nss $SO_4^=$ is responsible for the trend in increasing light scattering. However, a proxy for dust (non-sea salt Ca^{+2}) does show an increase in mass concentration over the past 5 years. The frequency and intensity of Asian dust events have increased over the past several years and may help to explain the increasing dust concentrations at Barrow during the Arctic haze season. Also it may be that organics, for which we have no direct measurement, are increasing. Trace elements that allow for the determination of

dust concentrations during the 2003 Arctic haze season have been measured and will soon be included in the analysis shown in Figure 2.

CONCLUSIONS

This project has produced the longest reported record of simultaneously measured aerosol chemical and optical properties at Barrow, Alaska. The resulting data record identifies the chemical components responsible for observed changes in aerosol optical properties on seasonal time scales. Hence, it provides a link between aerosol sources, transport mechanisms, and aerosol effects.

Aerosol scattering and mass measurements indicate Arctic haze is once again increasing at Barrow. The driving force behind this change and the responsible chemical components are unknown at this point. However, the addition of trace element analysis for the 2003 Arctic haze season and beyond should help to determine the role of dust in this observed trend.

REFERENCES

Barrie, L.A., R.M. Hoff, and S.M. Daggupaty (1981), The influence of midlatitudinal pollution sources on haze in the Canadian Arctic, *Atmos. Environ., 15,* 1407–1419.

Barrie, L.A., M.P. Olson, and K.K. Oikawa (1989), The flux of anthropogenic sulphur into the Arctic from midlatitudes in 1979/80, *Atmos. Environ., 23*, 2505–2512.

Delene, D.J., and J.A. Ogren (2002), Variability of aerosol optical properties at four North American surface monitoring sites, *J. Atmos. Sci., 59*, 1135–1150.

Heintzenberg, J., and S. Larssen (1983), SO_2 and SO_4 in the Arctic: Interpretation of observations at three Norwegian Arctic-Subarctic stations, *Tellus, 35B,* 255–265.

Iversen, T., and E. Joranger (1985), Arctic air pollution and large scale atmospheric flows, *Atmos. Environ., 19,* 2099–2108.

Quinn, P.K., T.L. Miller, T.S. Bates, J.A. Ogren, E. Andrews, and G.E. Shaw (2002), A three-year record of simultaneously measured aerosol chemical and optical properties at Barrow, Alaska, *J. Geophys. Res., 107*(D11), 4130, doi:10.1029/2001JD001248.

University of Denver Fourier Transform Spectrometer

R. VAN ALLEN, F. J. MURCRAY, R. D. BLATHERWICK, AND T. M. STEPHEN
Department of Physics and Astronomy, University of Denver, Colorado 80208-0202

INTRODUCTION

Since November 1991, the University of Denver (DU) has operated a very high-resolution (~0.003 cm^{-1}), two-channel (HgCdTe and InSb) Fourier Transform Spectrometer (FTS) from the Network for the Detection of Stratospheric Change (NDSC) site at Mauna Loa Observatory (MLO) to obtain atmospheric transmission spectra in the infrared region of the solar electromagnetic spectrum. Initially, a Bomem DA3.002 FTS was employed that required considerable operator attention. Consequently, it was only operated routinely once a week at sunrise and more frequently when DU personnel were on site for maintenance or for special campaigns. The spectral regions routinely covered were 750-1250 cm^{-1} and 2400-3050 cm^{-1}, and vertical column densities of N_2O, O_3, HNO_3, HCl, and CHF_2Cl were retrieved from the data. In August 1995 this system was replaced with a Bruker 120HR system. The new system takes measurements twice daily when weather permits and is almost completely automated requiring an operator to fill the detector dewars with liquid nitrogen occasionally. With the installation of this instrument, additional spectral intervals were added permitting the retrieval of column densities for the additional molecules CH_4, C_2H_6, HCN, NO, NO_2, HF, and CO.

OPERATIONAL DIFFICULTIES

During the past 2 years, the interferometer suffered a number of hardware problems that greatly reduced the amount of data acquired. In an attempt to correct these problems, DU personnel were dispatched to MLO several times during 2002 and in March, April, and July 2003 with an additional trip scheduled for December. Virtually all of the circuit boards and several mechanical components were replaced, and the short wavelength (InSb) channel is operating normally. The long wavelength (HgCdTe) channel continues to be a problem but should be operational soon. The data were analyzed in Denver for vertical column amounts of O_3, N_2O, CO, CH_4, NO, NO_2, HF, HCl, HNO_3, HCN, CHF_2Cl, C_2H_2, and C_2H_6, and the results of these analyses were placed in the NDSC archive.

ANALYSIS

The analysis was performed using the computer code SFIT [*Rinsland et al.,* 1984], that minimizes the root mean square (RMS) residual between a simulated spectrum and the observed spectrum by multiplying an assumed vertical volume mixing ratio profile by a scaling factor. The present analysis employed the HITRAN 96 spectral line parameter data base [*Rothman et al.,* 1998] along with pressure-temperature profiles from the daily National Weather Service (NWS) radiosondes launched from Hilo, Hawaii.

DATA REPROCESSING

It was recently discovered that the times assigned to coadded (averaged) interferograms were in error by ~35 seconds. Although this time offset has an insignificant effect on measurements performed at high sun (zenith angles $<60^o$), it does effect low sun (zenith angles $>75^o$) measurements by a few percent. Consequently, the effected data was either reprocessed or a correction was applied to the measured vertical column densities, and the archived data was changed accordingly.

CONCLUSION

We have a 12-year record for O_3, HNO_3, N_2O, HCl, and CHF_2Cl (F-22), and an 8-year record for CH_4, C_2H_6, HCN, NO, NO_2, HF, and CO. Although the instrument was not fully operational during much of the past year, we anticipate these difficulties will be resolved by early 2004.

Acknowledgments. This research was partially supported by NASA under grants NAG 2-1391 and NAG 2-1616. The collection of the data was done with the aid and support of CMDL. We are especially grateful to Bob Uchida for maintaining the experiment over the years.

REFERENCES

Rinsland, C.P., R.E. Boughner, J.C. Larsen, G.M. Stokes, and J.W. Brault (1984), Diurnal variations of atmospheric nitric oxide: Ground-based infrared spectroscopic measurements and their interpretation with time-dependent photochemical model calculations, *J. Geophys. Res., 89*, 9613-9622.

Rothman, L.S., C.P. Rinsland, A. Goldman, S.T. Massie, D.P. Edwards, J.-M. Flaud, A. Perrin, C. Camy-Peyrey, V. Dana, J.-Y. Mandin, J. Schroeder, A. McCann, R.R. Gamache, R.B. Wattsin, K. Yoshino, K.V. Chance, K.W. Juck, L.R. Brown, V. Nemtchechin, and P. Varanasi (1998), The HITRAN molecular spectroscopic database and HAWKS (HITRAN Atmospheric Work Station): 1996 Edition, *J. Quant. Spectrosc. and Radiat. Transfer, 60*, 665-710.